JGR Planets

RESEARCH ARTICLE

10.1029/2024JE008928

Temporal Changes in Europa's Ice Shell Thickness: Insights From Models of Convection

Ji-Ching Chen (Livia)[1,2], Frédéric Deschamps[1], and Wen-Pin Hsieh[1]

[1]Institute of Earth Sciences, Academia Sinica, Taipei, Taiwan, [2]Now at Seismological Laboratory, Division of Geological and Planetary Sciences, California Institute of Technology, Pasadena, CA, USA

Key Points:

- The thickness of Europa's ice shell (20–45 km) is predominantly influenced by tidal heating (~1 TW) and ice shell viscosity (~10^{14} Pa·s)
- Variations in Europa's orbital eccentricity (±10%) can induce changes of approximately 25 km in ice shell thickness
- The study reconciles ice thickness estimates from impact basin morphology and those based on Europa's thermal history modeling

Supporting Information:

Supporting Information may be found in the online version of this article.

Correspondence to:

J.-C. Chen (Livia) and F. Deschamps,
ching602504@gmail.com;
jcchen2@caltech.edu;
frederic@earth.sinica.edu.tw

Citation:

Chen (Livia), J.-C., Deschamps, F., & Hsieh, W.-P. (2026). Temporal changes in Europa's ice shell thickness: Insights from models of convection. *Journal of Geophysical Research: Planets*, *131*, e2024JE008928. https://doi.org/10.1029/2024JE008928

Received 14 JAN 2025
Accepted 30 DEC 2025

Author Contributions:

Conceptualization: Ji-Ching Chen (Livia), Frédéric Deschamps
Formal analysis: Ji-Ching Chen (Livia), Frédéric Deschamps
Funding acquisition: Frédéric Deschamps, Wen-Pin Hsieh
Methodology: Frédéric Deschamps
Project administration: Frédéric Deschamps, Wen-Pin Hsieh
Resources: Frédéric Deschamps
Supervision: Frédéric Deschamps, Wen-Pin Hsieh
Validation: Ji-Ching Chen (Livia), Frédéric Deschamps
Visualization: Ji-Ching Chen (Livia)

Abstract Europa is characterized by a thin ice I_h shell overlying a subsurface ocean and a large solid core. Estimates of the outer ice shell's thickness range from a few kilometers to several tens of kilometers, with strong implications for Europa's thermal and geological history. Here, we model the thermal evolution of Europa's ice shell using a parameterized convection approach that explicitly accounts for internal heat release. We explore changes in the thickness of this ice shell as a function of ice reference viscosity, tidal heating, and ocean composition. We further consider the effect of cyclical variations in tidal heating in response to changes in the eccentricity of Europa's orbit. Our calculations show that the ice shell thickness is mostly influenced by both the ice viscosity and tidal heating. While significant in the absence of tidal heating, the ocean composition has no or little influence when such heating is accounted for. For dissipated tidal power and viscosity around 1 TW and 10^{14} Pa·s, respectively, which are within the expected range of values for these parameters, our calculations predict an ice shell thickness in the range of 20–45 km including, at the top part of this shell, a stagnant lid ~10 km in thickness. These values are in agreement with recent estimates of impact basin morphology. Our calculations further indicate that a 10% change in orbital eccentricity may trigger variations in the ice shell thickness of approximately 15 km, which further helps to reconcile estimates based on geological features and modeled thermal history.

Plain Language Summary Europa has a thin ice layer covering a deep ocean and rocky core. A key question is how thick this ice layer is, with current estimates ranging from a few kilometers to over 50 km. This thickness is important for understanding Europa's history and how it cools down. We investigate factors that affect Europa's ice shell thickness and its evolution, including subsurface ocean composition, rheology (ice viscosity), and internal tidal heating on the ice shell. We also considered how changes in the tidal forces exerted by Jupiter, driven by orbital eccentricity, impact the ice shell over time. Our findings show that tidal heating and ice viscosity strongly affect the thickness of the ice shell, whereas the ocean's composition has a smaller effect. We further observed that temporal changes in the amount of tidal heat dissipated within Europa can lead to significant changes in the amplitude of the ice shell's thickness variation over time. Overall, our study helps refine estimates of how thick Europa's ice shell might be and shows that tidal heating plays a crucial role in shaping this ice layer. Importantly, this research bridges discrepancies between the surface geology features and those deduced from the modeling of Europa's thermal history.

1. Introduction

The structure of Europa's interior is believed to consist of a thin outer ice I_h shell covering a thick liquid subsurface ocean (Khurana, 1998; Kivelson et al., 2000), which is itself in direct contact with a large silicate core about 1,400 km in radius. Gravity measurements performed by the Galileo spacecraft suggest that the thickness of the entire hydrosphere, defined as the outer ice shell and the subsurface ocean, ranges from 135 to 185 km (Anderson et al., 1998; Gomez Casajus et al., 2021; Schubert & Spohn, 2004). The thickness of the outer ice shell is still a matter of debate, but is likely to range from a few kilometers to several tens of kilometers depending on the method used (Billings & Kattenhorn, 2005). Its evolution is affected by the thermal evolution of Europa, which, in turn, is predominantly controlled by several parameters, including the exact composition of the subsurface ocean, the efficiency of heat transfer within the outer ice shell and the available sources of heat (Hussmann & Spohn, 2004).

Three main sources of heat contribute to the energy budget: the secular cooling resulting from heat stored during accretion and differentiation; radiogenic heating in the silicate core; and tidal dissipation. Secular cooling and

Writing – original draft: Ji-Ching Chen (Livia), Frédéric Deschamps
Writing – review & editing: Ji-Ching Chen (Livia), Frédéric Deschamps, Wen-Pin Hsieh

radiogenic heating gradually decay over time and constitute a basal source of heat for the outer ice shell. Tidal dissipation is linked to the tidal forces exerted by Jupiter on Europa and primarily affects the outer ice shell (Běhounková et al., 2021; Howell, 2021; Hussmann & Spohn, 2004; Walker & Rhoden, 2022). The amount of tidal heating within the ice shell strongly affects the heat transfer through this region by limiting the heat that can be extracted from the subsurface ocean, which, in turn, impacts the ice shell evolution (Deschamps & Vilella, 2021; Hussmann & Spohn, 2004; Nimmo et al., 2007; Walker & Rhoden, 2022).

To date, available data do not allow constraining the ice shell thickness with precision (Billings & Kattenhorn, 2005). Different methods used to infer this thickness are sensitive to different parts or properties of the ice shell and to different temporal and spatial scales, resulting in a lack of consensus. Ice shell flexure analysis is sensitive to the elastic part of the shell at the moment observations are made, and usually suggests a very thin layer, from hundreds of meters up to ∼6 km thick (Hurford et al., 2005; Nimmo et al., 2003, 2007; Williams & Greeley, 1998). Structural methods, for instance based on ice rafts, mostly probe the brittle part of the ice shell under geologic stresses, thus reflecting the past active process rather than the present state. Again, these approaches suggest that Europa's ice shell is very thin, less than 6 km (Carr et al., 1998; Hoppa et al., 1999). Estimates deduced from impact cratering (Moore et al., 1998; Schenk, 2002; Silber & Johnson, 2017; Wakita et al., 2024) are based on the observed morphology (number of rings and the distances separating them) of impact basins, which depends on the thickness and rheology of the ice shell (Mc Kinnon & Melosh, 1980). These methods infer the ice shell thickness at a very specific moment (specifically, at the time of impact), and therefore do not necessarily reflect the current thickness. Using crater depth-to-diameter relationships, Schenk (2002) found that the ice shell is at least 19 km thick, including an 8 km brittle ice layer at its top. Based on the comparison between the observed morphology of large impact basins and that predicted by simulations of the deformation of an ice layer in response to such impacts, Silber and Johnson (2017) estimated that, if purely conductive, the ice shell should be around 8 km thick. If it overlies a layer of warm, viscous ice shell of unspecified thickness, this conductive lid reduces to 5–7 km. More recently, Wakita et al. (2024), also comparing observed impact basin morphology with results from numerical simulations, proposed that the ice shell may be at least 20 km thick, and that it consists of a 6−8 km brittle layer overlying a thicker viscous shell. The Europa Clipper mission, which will start exploring Europa in 2031, is expected to bring key observational constraints on Europa's ice shell thickness using different instruments and methods (Roberts et al., 2023). Magnetic data should give access to the subsurface ocean electrical conductivity and thickness (Kivelson et al., 2023). Note that the modeling of Galileo magnetic data (Schilling et al., 2007) estimated the ocean electrical conductivity and thickness to be 0.5 S/m and 100 km (i.e., a 60 km ice shell), respectively, but that the solutions of this modeling are non-unique. Gravity measurements will measure Europa's tidal Love numbers, whose value depends on the presence and thickness of a subsurface ocean (Mazarico et al., 2023). The k_2, for instance, is expected to range from less than 0.015 if no ocean is present to about 0.22 for a 10 km thick ice shell (150 km ocean). Finally, radar sounding will be able to detect an ice/ocean boundary up to 30 km beneath the surface of Europa (Blankenship et al., 2024).

Besides estimates based on the analysis of surface observation, models of Europa's thermal evolution have been used to estimate Europa's outer ice shell thickness (Běhounková et al., 2010; Deschamps & Sotin, 2001; Deschamps & Vilella, 2021; Green et al., 2021; Han & Showman, 2010; Howell, 2021; Hussmann, 2002; Hussmann & Spohn, 2004; Nimmo et al., 2003). These methods involve a much longer timescale than the methods based on the interpretation of surface geological features. However, they do not make clear predictions for the geological structure that may be present today, such that it is difficult to compare the thickness they predict against available data and observations. In addition, thermal equilibrium models usually provide an average thickness and do not constrain possible lateral variations in this thickness. Calculations point to a rather thick ice shell, from about 15 km to several tens of kilometers. Importantly, the predicted thickness strongly depends on the assumed ice properties (in particular its viscosity), and on the heat released within the ice shell. It is also worth noting that the generation of pockets of melted ice, which is needed to explain cryo-volcanism, requires an ice shell thickness in the range of 15−35 km (Vilella et al., 2020).

Here, we model the thermal evolution of Europa's outer ice shell using scaling laws for heat flux and temperature that explicitly account for the release of heat within this shell. We explore the influence of key parameters, including the ice reference viscosity, the amount of heat dissipated within the ice shell, and the composition of the subsurface ocean. A novelty, compared to previous models, is that we investigate the roles played by the time-dependent tidal dissipation, and by distributing tidal heating within the core and the ice shell. For reasonable

Table 1
Properties of Europa and Its Interior Materials

Parameter	Unit	Value or expression	Symbol
Global parameters of Europa			
Total radius	km	1,561	R
Core radius	km	1,400	r_c
Gravity acceleration	$m{\cdot}s^{-2}$	1.31	g
Surface temperature	K	100	T_s
Reference thermal conductivity	$W{\cdot}m^{-1}K^{-1}$	2.6	k_{ref}
Orbital frequency	s^{-1}	2.05×10^{-5}	ω
Ice I_h			
Density	$kg{\cdot}m^{-3}$	920	ρ_I
Thermal conductivity	$W{\cdot}m^{-1}K^{-1}$	566.8/T	k_I
Thermal expansivity	K^{-1}	1.56×10^{-4}	α_I
Heat capacity	$J{\cdot}kg^{-1}K^{-1}$	7.037 T + 185	C_I
Latent heat of fusion	$kJ{\cdot}kg^{-1}$	284	L_I
Rigidity	G·Pa	4	μ_I
Reference viscosity	Pa·s	$10^{13} - 10^{15}$	η_{ref}
Activation energy	$kJ{\cdot}mol^{-1}$	60	E
Liquid water + impurities			
Density of water	$kg{\cdot}m^{-3}$	1,000	ρ_w
Density of ammonia	$kg{\cdot}m^{-3}$	734	ρ_{NH_3}
Thermal expansivity of water	K^{-1}	3×10^{-4}	α_w
Heat capacity of water	$J{\cdot}kg^{-1}K^{-1}$	4,180	C_w
Silicate core			
Density	$kg{\cdot}m^{-3}$	3,300	ρ_c
Thermal diffusivity	m^2s^{-1}	10^{-6}	κ_c
Thermal conductivity	$W{\cdot}m^{-1}K^{-1}$	4.0	k_c
Heat capacity	$J{\cdot}kg^{-1}K^{-1}$	1,200	C_c

values of the tidal heating and ice reference viscosity, our calculations predict a range of ice shell thickness that is in good agreement with the estimates deduced from the morphology of impact basins.

2. Method

To model Europa's thermal evolution, we used a parameterized convection approach based on scaling laws describing the thermal properties (heat flux, average temperature, and stagnant lid thickness) of the outer ice shell (Section 2.1) and solving the energy balance at the interface between the ice shell and the subsurface ocean (Section 2.4). The method we used is mostly similar to that in Deschamps and Vilella (2021). A major difference, however, is that we take into account time-variations in the amount of tidal heating due to Europa's orbital evolution (Section 2.5). Another difference is the treatment of the core's thermal evolution (in response to radiogenic heating), which now consists of solving the heat equation instead of using Kirk and Stevenson (1987)'s approximation (Section 2.3). This further allows adding tidal heating within the core and investigating its effect on Europa's evolution. The main aspects of our method are summarized in Sections 2.1–2.6. The values of physical and material properties used for calculations are listed in Table 1.

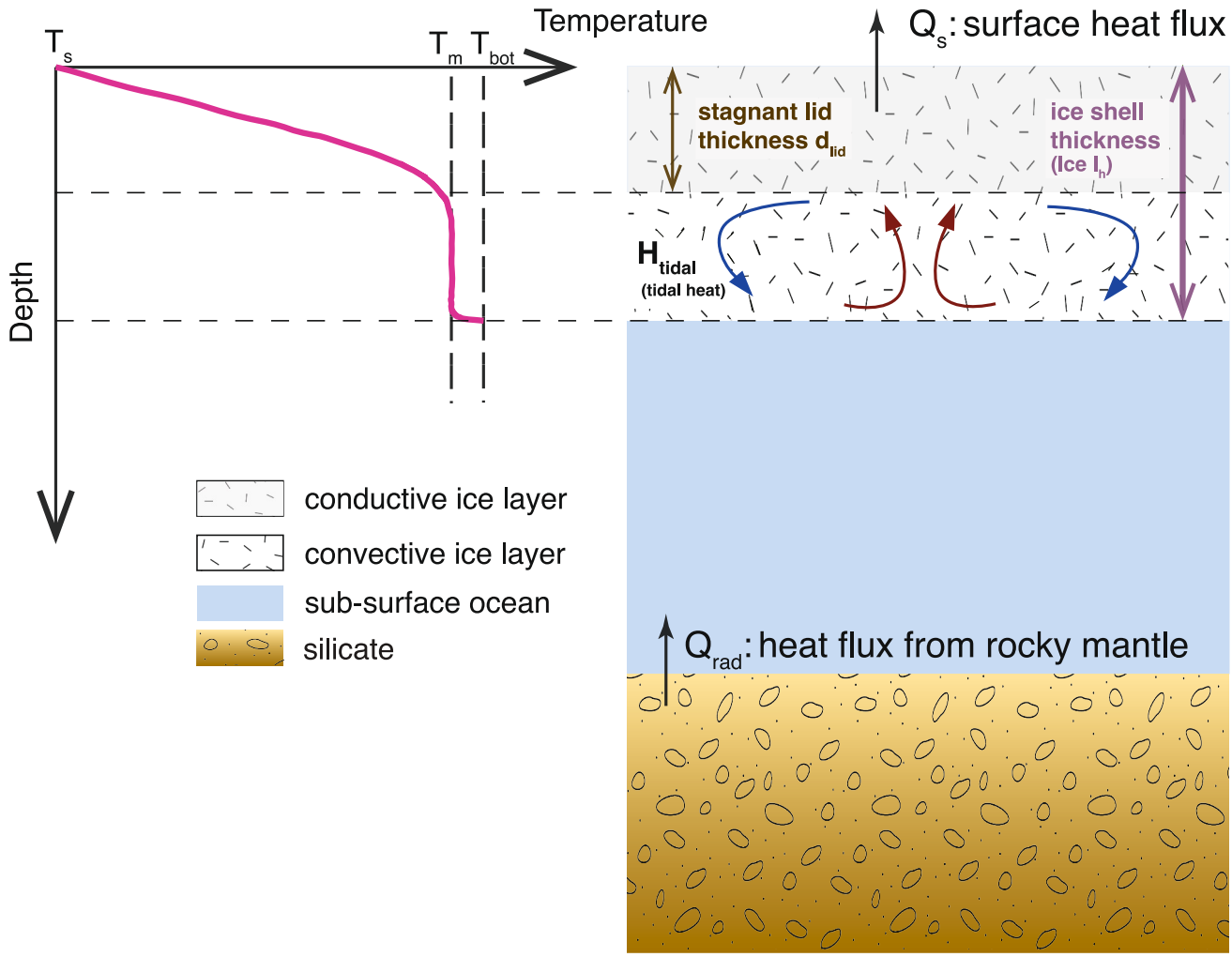

Figure 1. Schematic radial structure of the ice shell. The ice shell is divided into a conductive (or stagnant) lid of thickness d_{lid} (gray shaded area) overlaying an ice layer (white) animated by convection. Heat H_{tidal} is generated internally by tidal dissipation. Q_{rad} is the heat flux at the top of the core. To investigate the evolution of the ice shell properties (average temperature, total and stagnant lid thickness, bottom heat flux), our model solves the heat balance equation at the boundary between the ice shell and the subsurface ocean using scaling laws derived from simulations of convection. The surface temperature, T_s, is an input parameter here fixed to 100 K, while the interior and bottom temperatures, T_m and T_{bot}, are given by Equation 3 and the liquidus of the water + ammonia, respectively. The red curve schematically illustrates the radial temperature profile within the ice shell and is not based on specific numerical values.

2.1. Outer Ice Shell

The outer ice shell is composed of ice I_{h} and transfers heat either by conduction or by convection, depending on its properties. Because the viscosity of ice I_{h} strongly depends on temperature (e.g., Durham et al. (2010)), convection in the ice shell operates in the stagnant lid regime, in which a rigid, thermally conductive lid forms at the top of the shell and convection is confined beneath this lid (Figure 1). As a result, heat transfer is less efficient and the cooling is delayed. The surface of the ice shell is held at a constant temperature, T_s, while its base is a dynamic boundary representing the interface between the solid ice shell and the liquid subsurface ocean, where the temperature T_{bot} is defined as the melting point of water with (if present) impurities. For simplicity, we do not account for the presence of a mushy layer at the ice-water interface (Buffo et al., 2021), which, together with the presence of a basal layer of volatiles (as assumed in the case of Pluto, Kamata et al. (2019)), may act as a thermal insulator between the ice shell and the subsurface ocean (see discussion). Throughout the model's evolution, the thickness of the ice shell varies in response to Europa's cooling. We fixed the initial layer thickness to 10 km (Section 2.6) and determined its evolution by solving the energy conservation equation at the boundary between the shell and the subsurface ocean (Section 2.4).

We describe the viscosity of ice I_h with

$$\eta(T) = \eta_{ref} \exp\left[\frac{E}{R_g T_{ref}}\left(\frac{T_{ref}}{T} - 1\right)\right], \quad (1)$$

where E is the activation energy of ice, R_g is the ideal gas constant and η_{ref} is the ice reference viscosity, defined as the viscosity close to the ice melting point, at temperature T_{ref}. In all our calculations, T_{ref} is fixed to 270 K. Different creep mechanisms may affect the deformation of ice depending on temperature, pressure and strain rate. Creep data extrapolated from polar ice sheets and mountain glaciers (Montagnat & Duval, 2000) suggest that ice exhibits a Newtonian fluid behavior at low strain rates (equation image $<10^{-11}$ s^{-1}). In order to maintain a simple thermodynamical framework, we neglect the complexities of rheology such as the ice porosity, non-Newtonian creep and grain size effects. The value of η_{ref} is poorly known, leading to a large uncertainty on the ice shell viscosity, and subsequently on its evolution (see result section). Close to the ice melting point, the ice viscosity is usually assumed to be in the range of 10^{13}–10^{15} Pa·s. Activation energy, which controls the temperature-dependence of the viscosity, is better constrained, with values ranging from 56 to 63 kJ/mol depending on the type of diffusion mechanism (Goldsby & Kohlstedt, 2001; Howell, 2021), and approximately 60 kJ/mol for atomic diffusion (Weertman, 1983). The activation energy of ice implies that its viscosity is strongly temperature-dependent, suggesting that convection in Europa's ice shell operates in the stagnant-lid regime (e.g., Davaille & Jaupart, 1993; Moresi & Solomatov, 1995; Ogawa et al., 1991). Here, we use $E = 60$ kJmol^{-1} in all our calculations. Higher (lower) values of E would result in stronger (weaker) temperature-dependences, and thus stronger (weaker) stagnant lids.

We determine the thermal properties of the outer ice shell using the scaling laws for surface heat flux, Q_S, internal temperature, T_m, and stagnant lid thickness, d_{lid}, defined by Deschamps and Vilella (2021). These scalings were obtained from simulations of convection in an incompressible, mixed (i.e., both basally and internally) heated fluid. As both the interior temperature and the thickness of ice change with time, the layer's heat balance changes at every time-step, providing a description of the thermal and radial structure of the outer ice shell. At each timestep, we determine the properties of the shell as follows:

Interior temperature. The interior temperature parameterization is described by a relationship combining for interior temperature parameterizations obtained for purely basally heated stagnant lid convection (Deschamps & Lin, 2014; Yao et al., 2014), and for purely internally heated isoviscous convection (Deschamps et al., 2010; Sotin & Labrosse, 1999). In its non-dimensional form, the temperature scaling writes

$$\widetilde{T}_m = 1 - \frac{a_1}{f^{a_2}\gamma} + (c_1 + c_2 f)\left[\frac{(1+f+f^2)}{3}\widetilde{H}\right]^{c_4} \frac{1}{Ra_{eff}{}^{c_3}}, \quad (2)$$

where the non-dimensional temperature and heating rate per unit mass, $\widetilde{T}$ and $\widetilde{H}$, are related to their dimensional values, T and H, by $\widetilde{T} = (T - T_{top})/\Delta T$ and $\widetilde{H} = \rho_I H D^2/k_I \Delta T$, respectively, with $\Delta T = (T_{bot} - T_{top})$ being the super-adiabatic temperature jump, T_{bot} the bottom temperature (defined here as the liquidus of a mix of water and impurities), T_{top} the surface temperature, ρ_I and k_I the density and thermal conductivity of ice I_h, and D the thickness of the ice shell. The first two terms in Equation 2 represent the interior temperature for basally heated stagnant lid convection, where viscosity changes with temperature are accounted for by the parameter γ, defined as the inverse of the non-dimensional viscous temperature scale, $\Delta T_v/\Delta T$. The third term describes the effect of internal heating. Note that this term depends on the effective Rayleigh number, Ra_{eff} (which we define below, Equation 4). Both the basally and internally heated terms are influenced by the ice shell's curvature, here controlled with the ratio between the inner and outer shell radii, f. Finally, the parameters $a_1 = 1.23$, $a_2 = 1.5$, $c_1 = 3.5$, $c_2 = -2.3$, $c_3 = 0.25$ and $c_4 = 1$ were obtained by inversion of values of $\widetilde{T}_m$ predicted by numerical simulations of stagnant lid convection (Deschamps & Vilella, 2021). Rescaling Equation 2 further requires the definition of a viscous temperature scale, which, if viscosity is described with Equation 1, is given by $\Delta T_v = R_g T_m{}^2/E$. The (dimensional) interior temperature can then be described with

$$T_m = T_{\text{bot}} - \frac{a_1}{f^{a_2}} \frac{RT_m{}^2}{E} + (c_1 + c_2 f) \left[\frac{(1 + f + f^2)}{3} \frac{\rho_I H D^2}{k_I \Delta T} \right]^{c_4} \frac{\Delta T}{Ra_{\text{eff}}{}^{c_3}}, \tag{3}$$

where the Rayleigh number Ra_{eff} quantifies the vigor of convection within the ice shell and is calculated using the viscosity at temperature T_{m} following

$$Ra_{\text{eff}} = \frac{\alpha_I \rho_I g \Delta T D^3}{\eta(T_m)\, \kappa_I}. \tag{4}$$

In Equation 4, α_I and κ_I are the thermal expansion and thermal diffusivity of ice I_{h}, and the viscosity at internal temperature, $\eta\,(T_{\text{m}})$, is calculated using Equation 1. Equation 3 does not have an analytical solution, and we solved it using a Newton-Raphson zero-search method (Press et al., 1992).

Surface heat flux. The surface heat flux scales as a power law of the Rayleigh number and of the temperature jump across the thermal boundary layers. For stagnant lid convection, this implies that it scales as the inverse of the non-dimensional viscous temperature scale $\gamma = \Delta T/\Delta T_{\text{v}}$. Therefore, the nondimensional surface heat flux can be expressed as a function of the Rayleigh number and the viscous temperature scale (Deschamps & Lin, 2014; Yao et al., 2014),

$$\widetilde{Q}_{\text{top}} = a \frac{Ra_{\text{eff}}^b}{\gamma^c}, \tag{5}$$

where the values of constants a, b, and c were again obtained by inverting heat flux predicted by simulations of convection (Yao et al., 2014), and are equal to 1.46, 0.27, and 1.21, respectively. While these values were obtained for pure bottom heated cases, they do not depend on the amount of internal heating (Deschamps & Vilella, 2021), and are also valid for mixed-heated convection. By contrast, the bottom heat flux depends on the amount of internal heating dissipated in the ice shell, with larger internal heating reducing the bottom heat flux, that is, the amount of heat that can be extracted from the subsurface ocean. Interestingly, Equation 5 also describes cases where internal heating is not distributed homogeneously in the shell, for instance due to changes in viscosity (Deschamps & Vilella, 2021). In spherical geometry, the characteristic heat flux is $Q_{\text{charac}} = k_{\text{ref}} \Delta T/D$, where k_{ref} is the reference thermal conductivity, which we here fix to 2.6 W/m/K (Grasset & Sotin, 1996). Accounting for the shell's curvature, measured using f, and applying energy conservation, the basal and surface heat fluxes write

$$Q_s = Q_{\text{charac}} \widetilde{Q}_{\text{top}} \tag{6}$$

and

$$Q_{\text{bot}} = Q_s/f^2 - \frac{(1 + f + f^2)}{3f^2} H. \tag{7}$$

Note that if the surface heat flux is lower than the conductive characteristic heat flux, Q_{charac}, the system is not animated by convection and transfers heat by conduction. This occurs, for instance, if the ice shell is too thin, if the viscosity of this shell is too large, or if the concentration of impurities in the subsurface ocean is too high. In the latter case, the bottom temperature of the shell is significantly lower than that of a pure water ocean. Consequently, both the reference and interior viscosities increase, reducing the vigor of convection or even completely halting it (Deschamps & Sotin, 2001).

Stagnant lid thickness. Since in the stagnant lid heat is transported by conduction, it is possible to derive analytical expressions for the horizontally averaged temperature within this lid by solving the conduction heat equation. Assuming that the internal heating rate and the density are constant and that the surface temperature and heat flux are known, the dimensional temperature profile is given by

$$T(r) = T_{\text{surf}} - \frac{Q_s}{k_I} R\left(1 - \frac{R}{r}\right) + \frac{\overline{\rho_I} H R^2}{6 k_I}\left[2\left(1 - \frac{R}{r}\right) + \left(1 - \frac{r^2}{R^2}\right)\right], \quad (8)$$

where T is the temperature at radius r, R is the total radius, k_I the thermal conductivity, $\overline{\rho_I}$ the ice density and H the internal heating rate per unit mass. Note that the thermal conductivity of ice depends on temperature, which may affect the thermal structure of the stagnant lid and increase its thickness (Deschamps, 2020). Here, we did not take this effect into account. Comparisons between numerical simulations show that Equation 8 well describes the average temperature profile in the stagnant lid (Deschamps & Vilella, 2021). However, it is difficult to determine the boundary between the stagnant lid and the top of the thermal boundary layer. Noting that the thickness of this lid should approximately scale as the inverse of the heat flux leads to (Deschamps & Vilella, 2021)

$$d_{\text{lid}} = \frac{a_{\text{lid}} \gamma^c}{Ra_{\text{eff}}{}^b} D, \quad (9)$$

where the values of parameters b and c are identical to those of the surface heat flux (i.e., $b = 0.27$ and $c = 1.21$), a_{lid} is a constant equal to 0.633, and D the thickness of the ice shell. The value of a_{lid} was, again, determined by fitting stagnant lid thicknesses deduced from numerical simulations, the lid thickness being estimated by the intersection between the tangent at the point of inflexion of the horizontally averaged profile of vertically advected heat with the origin axis (see Deschamps & Vilella, 2021 for details). Following Equation 9, the thickness of the stagnant lid reflects the strength of the temperature dependence of viscosity, with stronger dependence (larger γ) leading to a thicker lid. Since $\gamma = \Delta T/\Delta T_{\text{v}}$ and $\Delta T_v = R_g {T_m}^2/E$, the thickness of the lid strongly depends on the interior temperature, which is itself partly controlled by the bottom temperature (Equation 3), with lower temperatures (and thus, lower liquidus) leading to thicker lids. Finally, following Equation 8 and given the lid thickness, the temperature at the bottom of the stagnant lid can be calculated following

$$T_{\text{lid}} = T_{\text{surf}} + \frac{d_{\text{lid}}}{k f_{\text{lid}}}\left[Q_s - \frac{\overline{\rho} H R}{6}\left(2 - f_{\text{lid}} - f_{\text{lid}}^2\right)\right], \quad (10)$$

where $f_{\text{lid}} = (R - d_{\text{lid}})/R = 1 - (1 - f)\, d_{\text{lid}}/D$ is the ratio between the radius of the base of the lid and the surface radius.

2.2. Subsurface Ocean

The subsurface ocean is assumed to be adiabatic, such that the heat available at the bottom of the ice shell is equal to the heat (essentially radiogenic) released from the core. In the case of thin oceans, tidal heat dissipation may also be important (Tyler, 2014). This would increase the available heat at the bottom of the ice shell, thereby delaying the crystallization of the remaining ocean. However, because under such conditions the ice shell would be very thick, heat transfer in this shell would be overall more efficient and extract more heat from the ocean. Also, anticipating our results (Section 3), the dissipation of substantial amounts of heat (~0.5 TW and more) prevents the crystallization of a thick shell. Europa's subsurface ocean is mainly composed of water plus small amounts of impurities. Its exact composition is not constrained but likely includes salts such as sodium chloride (NaCl) and magnesium sulfate ($MgSO_4$), and volatile compounds such as ammonia (NH_3), methanol (CH_3OH) and methane (CH_4) (Carlson, 1999; Trumbo et al., 2019). These compounds act as anti-freeze, that is, they oppose or delay the crystallization of the subsurface ocean, and may further influence the dynamics of the ice shell (Deschamps & Sotin, 2001). Salts, in particular $MgSO_4$, are likely a key component of the subsurface ocean (Becker et al., 2024), but to date, there is no detailed experimental phase diagram for water + $MgSO_4$ mixtures. Here, we therefore focus on the effect of ammonia, which is expected to condense in environments of giant planets with predicted concentrations reaching up to a few weight percent (Mousis et al., 2009), and for which a detailed experimental phase diagram is available (Sotin et al., 1997). Note that using other compounds may impact details of the crystallization process and thermal evolution but would not qualitatively modify them. Different amounts of different compounds may further lead to similar evolutions. For instance, Vilella et al. (2020) pointed out that the effect of 30% $MgSO_4$ is similar to that of 5.0 wt% NH_3. Furthermore, anticipating again our results (Section 3), the role of anti-freeze compounds has no or very small influence if large amounts of

heat are dissipated in the ice shell. Changes in the ice shell thickness trigger changes in the concentration of impurities. Up to the eutectic composition (which, for a mixture of water and ammonia, is equal to 32.2 wt% of NH_3), only water crystallizes, leaving impurities in the ocean. As a result, the concentration of ammonia (and more generally of impurities) in the remaining ocean is increasing as the ice shell thickens. For calculations, we fixed the initial fraction of ammonia and we updated the concentration at each timestep following $x^{\mathrm{vol}}_{\mathrm{NH3}} = x^{\mathrm{vol}}_{\mathrm{NH3,init}} V_{\mathrm{ocean,init}}/V_{\mathrm{ocean}}$, where $V_{\mathrm{ocean,init}}$ and V_{ocean} are the subsurface ocean initial and updated volumes. For convenience, calculations are conducted with volume fraction of ammonia, which we then adjust to weight fraction when determining the liquidus following (in the case of ammonia)

$$x^{\mathrm{wt}}_{\mathrm{NH_3}} = \frac{x^{\mathrm{vol}}_{\mathrm{NH3}} \rho_{\mathrm{NH_3}}}{x^{\mathrm{vol}}_{\mathrm{NH_3}} \rho_{\mathrm{NH_3}} + (1 - x^{\mathrm{vol}}_{\mathrm{NH_3}})\rho_w}, \tag{11}$$

where ρ_w and $\rho_{\mathrm{NH_3}}$ are the density of liquid water and ammonia, respectively. With this setup, and for initial ammonia concentrations of 1.5 and 3.0 vol%, the eutectic composition of the water-ammonia system is reached for an ice shell of about 154 and 145 km, respectively, that is, very close to a full crystallization of the initial ocean. In practice, such thicknesses are obtained only if the reference viscosity is around 10^{13} Pa·s or less and if no tidal heating is dissipated in the ice shell (see Results section), and therefore the subsurface ocean is never close to a eutectic composition if internal heating is included and/or a more realistic reference is assumed. Finally, it is worth mentioning that the temperature at the bottom of the ice shell is determined at the melting point of pure water mixed with impurities, while the melting point within the ice shell is imposed by the melting temperature of pure water.

2.3. Silicate Core

The core is assumed to be composed of silicate rocks. Its radius is fixed at 1,400 km, leading to a hydrosphere of 161 km. The radial thermal structure of the core $T_c\ (r)$ and the heat flux at its top, Q_c, are calculated by solving the time-dependent heat diffusion equation,

$$\rho_c C_c \frac{dT_c}{dt} = \frac{1}{r^2}\frac{d}{dr}\left(r^2 k_c \frac{dT_c}{dr}\right) + H_c(t), \tag{12}$$

where r_c, C_c and k_c are the density, specific heat, and thermal conductivity of the core, respectively. Solving Equation 12 requires the prescription of the core surface temperature, which is here calculated from the temperature at the bottom of the ice shell, T_{bot}, and the assumption that the subsurface ocean is adiabatic (Section 2.4 and Equation 15; in practice, and given parameters in Table 1, the temperature at the top of the core is nearly identical to T_{bot}). The cooling of the core (and the evolution of Q_c) thus implicitly depends on the ice shell evolution. The volumetric heating, H_c, is caused by radiogenic heating H_{rad} due to the decay of isotopes ^{235}U, ^{238}U, ^{232}Th and ^{40}K with chondritic concentration (Lodders, 2003). The radiogenic heat produced at time t is given by

$$H_{\mathrm{rad}}(t) = \sum_{i=1,4} H_i C_{0,i} e^{-\lambda_i t}, \tag{13}$$

where H_i is the heat release per mass unit, $C_{0,i}$ the initial concentration and λ_i the decay constant for element i (Table 2). The total radiogenic power as a function of time (green dashed curve in Figure 2a) is simply given by H_{rad} (Equation 13) multiplied by the core volume and density. An example of core top heat flux is shown in Figure 2b. To estimate the influence of distributing tidal heating between the ice shell and the core, we also run calculations in which part of the volumetric heating is due to tidal heating. In that case, the core total power and top heat flux would be similar to those plotted in Figure 2 to which small oscillations are added.

2.4. Thermal Evolution

We calculate the evolution of the ice shell thickness by solving the energy conservation at the boundary between the top of the subsurface ocean and the bottom of the ice shell (ice/ocean interface), which writes

Table 2
Properties of Long-Lived Radioactive Isotope Parameters

Element	Initial concentration (10^{-9} kg/kg)	Heat release (W/kg)	Decay constant (1/yr)
^{235}U	5.4	5.687×10^{-4}	9.8485×10^{-10}
^{238}U	19.9	9.465×10^{-5}	1.5514×10^{-10}
^{232}Th	38.7	2.638×10^{-5}	4.9405×10^{-11}
^{40}K	738.0	2.917×10^{-5}	5.4279×10^{-10}

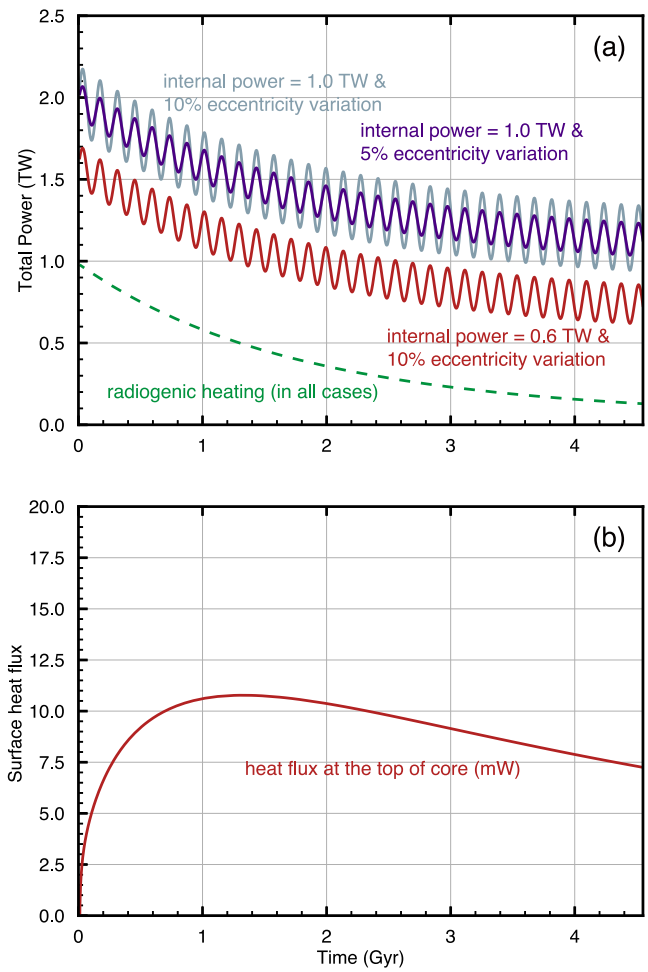

Figure 2. (a) Power produced by tidal dissipation for different assumptions (grayish blue, red, and purple curves) and radiogenic heating in the core (green dashed curve). Time-dependent tidal heating is due to a periodically varying eccentricity and is calculated following Equation 16. (b) Heat flux at the surface of the core and the core temperature deduced from solving the heat diffusion equation. The ice reference viscosity is 10^{14} Pa·s, and the period and amplitude of the variations in the orbit's eccentricity are fixed at 0.14 Gyr and 10% with a tidal power $P_0 = 0.6$ TW.

$$\frac{dr_{\rm bot}}{dt}\left[\rho_w C_w\left(-\frac{\partial T_{\rm ad}}{\partial r}+\frac{\partial T_{\rm bot}}{\partial r}\right)\frac{\left({r_{\rm bot}}^3-{r_c}^3\right)}{3}-\rho_I L_I {r_{\rm bot}}^2\right] = {r_{\rm bot}}^2 Q_{\rm bot}-{r_c}^2 Q_c, \quad (14)$$

where $r_{\rm bot}$ is the radius of the ice/ocean interface, t is time, $T_{\rm bot}$ and $Q_{\rm bot}$ are the temperature and heat flux at the bottom of the ice layer, given by the liquidus of the ocean and by Equation 7, respectively, r_c is the core radius, Q_c the heat flux at the top of the core (Section 2.3), ρ_w and C_w are the liquid water density and heat capacity, ρ_I and L_I the density and latent heat of ice $I_{\rm h}$, and $T_{\rm ad}$ is the adiabatic temperature in the ocean, given by

$$T_{\rm ad}(r) = T_{\rm bot}(r_{\rm bot})\left[1-\frac{\alpha_w}{\rho_w C_w}\rho_I g(r-r_{\rm bot})\right] \quad (15)$$

with α_w being the thermal expansion of liquid water. We solve Equation 14 forward in time up to 4.55 billion years (Gyr) using an adaptative step-size control Runge-Kutta method (Press et al., 1992), with parameters values listed in Table 1. By definition, the bottom temperature, $T_{\rm bot}$, is given by the phase diagram of the water mixed with impurities (here, ammonia) system. As this temperature changes with time, the ice shell thickens or thins.

Our approach therefore follows a classical Stefan problem, which describes the movement of a phase-change boundary assuming that the materials on both sides of the boundary are stationary, and that thermochemical properties remain constant. In natural systems, however, complexities may arise. For instance, the classical Stefan problem assumes that the temperature at the phase-change boundary immediately adjusts to the new physical conditions (e.g., pressure) at this boundary, which, in practice, does not happen. In addition, the thermal properties of ice and water at the boundary may vary during the phase change and modify the kinetics of the phase change. More importantly, in the case of icy moons, the subsurface ocean may be flowing. The kinetic energy associated with this motion should then be accounted for in the energy balance (Equation 14), which would delay the crystallization of the ocean. Another possible complexity arising in icy moons is that the phase boundary may have a topography, in particular if the ice layer is animated by convection. In this case, ice flow would result in positive (upward) dynamic topography at plume locations and negative (downward) topography at downwellings. Lateral changes in heat flux may accentuate this topography, promoting crystallization at downwellings (where local heat flux is larger) and moderating it at plumes (where local heat flux is lower). The 1D classical Stefan problem may thus not capture all the complexity of icy moons' evolution.

2.5. Time-Dependent Tidal Heating

The strong tidal gravitational forces exerted by Jupiter on Europa trigger deformation of Europa's ice shell. In particular, strike-slip displacements are accompanied by frictional heating, which, in turn, results in the dissipation of heat (Allu Peddinti & McNamara, 2019; Běhounková et al., 2021; Gaidos & Nimmo, 2000; Howell, 2021; Nimmo & Gaidos, 2002). Dissipated heat acts as a source of internal heating, increasing the temperature of the ice shell and reducing the amount of heat flux that can be extracted at the bottom of this shell and transported to its surface (Deschamps & Vilella, 2021). Tidal dissipation increases with the orbital eccentricity. Today, Europa's orbital

eccentricity is equal to 0.0094, but due to gravitational interactions with Jupiter's other moons, it varies with time, resulting in time-dependent tidal heating. Because Europa is locked in a complex resonance with Io and Ganymede, the variations in its orbital eccentricity are irregular and most likely non-periodic. The amplitude of long-term variations in Europa's eccentricity are not well constrained, and available estimates depend, in particular, on the assumed resonances between the Galilean moons. The calculations of Hussmann and Spohn (2004), which couple thermal and orbital evolutions, suggest variations of ∼60% around an average value of ∼0.024, while more recent simulations based on a dynamical orbital method (Lari et al., 2020) predict variations from 5% to 50%, depending on the assumed resonance chain and on the angle formed by the mean orbital longitudes of Galilean moons. The amount of heat released within Europa's interior further depends on its radial structure and on the viscosity of its internal layers (e.g., Beuthe, 2015), such that an accurate determination of the dissipated heat at a given time requires coupling thermal and orbital evolution. Here, for simplicity, we only consider the effects of time-dependent eccentricity, keeping in mind that structural parameters may also have an impact on the amount of heat dissipated. Also, for simplicity, we assume that the total tidal power P_{tide} varies periodically as a function of time following

$$P_{\text{tide}} = P_0 \left[a_0 + a_1 \sin \frac{2\pi t}{P} \right]^2, \tag{16}$$

where P_0 is the tidal power for the reference orbital eccentricity e_0, t is the time and P the period of orbital eccentricity variation. The constants a_0 and a_1 are related to the maximum and minimum eccentricity, e_{max} and e_{min}, respectively, and are given by

$$a_0 = \frac{(e_{\text{max}} + e_{\text{min}})}{2} \tag{17}$$

and

$$a_1 = \frac{(e_{\text{max}} - e_{\text{min}})}{2}. \tag{18}$$

With Equations 16–18, a 10% variation in eccentricity compared to the average eccentricity e_0 (i.e., $e_{\text{min}} = 0.9\, e_0$ and $e_{\text{max}} = 1.1\, e_0$) results in a peak-to-peak variation in tidal power equal to $0.4\, P_0$. Following Hussmann and Spohn (2004), we fixed the period to $P_0 = 0.14$ Gyr. As noted above, the choice to vary eccentricity using a periodic function is purely arbitrary and is not based on some observational or theoretical considerations. It may, however, be suitable for our goal here, which is to estimate the response of the outer ice shell to a given change in orbital eccentricity. Figure 2 illustrates variations of the total power (i.e., the radiogenic power produced in the core plus the tidal power) available in Europa as a function of time. The dissipated heat per unit mass (which is used, in particular, to calculate the internal temperature in Equation 3) within a layer of volume V and density ρ is simply given by $H = P/\rho V$.

Tidal dissipation may also affect the rocky core, entertaining hydrothermal activity within this core and volcanism at its surface (Běhounková et al., 2021). In that case, to fully describe the energy balance at the bottom of the ice shell, tidal dissipation should be added to the radiogenic power. To take this into account, we performed a few calculations in which the total power is split between the outer ice shell and the core with a fraction $x_{\text{tide}}^{\text{ice}}$ and $(1 - x_{\text{tide}}^{\text{ice}})$, respectively. Tidal heating within each of these regions is then estimated according to their volume and density. Again, one may point out that the total amount of heat dissipated and the distribution of this heat both depend on the radial structure and on the material properties (essentially, the viscosity) of the different layers. Because here our goal is only to assess the effect of distributing a given amount of heat between the ice shell and the silicate core, we simply prescribe the total amount of dissipated heat, which we then arbitrarily distribute between the ice shell and the core.

2.6. Initial Conditions

All calculations start with an initial ice shell thickness equal to 10 km. The initial temperature in the core is an isotherm corresponding to the temperature at the bottom of a 10 km ice shell. For an initial concentration in

ammonia equal to 1.5 wt%, this leads to a temperature of 272.5 K. We tested the influence of these initial conditions on the ice shell evolution, varying the initial thickness in the range of 5–20 km and the initial core isotherm up to 500 K (Figure S1 in Supporting Information S1). While initial thickness has a small impact on the early evolution of the shell, it leaves the properties of this shell unchanged in the long term. As one could expect, increasing the initial temperature has a strong effect in the early evolution stages of the ice shell and up to ∼1.0 Gyr by controlling the maximum shell thickness during these stages. Larger initial temperatures lead to thicker early shells, and an initial temperature of 500 K or higher prevents the growth of the ice shell. In the long term, however, differences are small, with higher initial temperature leading to a final ice shell thinner by only a few kilometers compared to our calculations.

3. Results

The individual impacts of internal heating, ice reference viscosity, and ocean composition follow general trends that can be summarized as follows. First, increasing the amount of tidal power triggers an elevation of temperature that delays ocean crystallization. This temperature increase further reduces the amount of heat that can be extracted from the subsurface ocean. Although a higher temperature reduces viscosity and therefore promotes convection, it also decreases the temperature contrast that drives buoyant plumes, thus weakening convection and decreasing the efficiency of heat transport (Deschamps et al., 2010; Sotin & Labrosse, 1999). Second, increasing reference viscosity reduces the vigor of convection, and thus, again, the ability of transferring heat toward the surface. Third, increasing the amount of anti-freeze compounds in the subsurface ocean reduces the temperature at the bottom of the outer ice shell, making the conditions for pursuing the crystallization more challenging. In addition, this cooling leads to an overall increase in bottom viscosity, which weakens convection, and to a stronger sensitivity of viscosity to temperature through the viscous temperature scale (Section 2.1), which strengthens the stagnant lid, further weakening convection and reducing heat extraction from the ocean and heat transfer through the ice shell. Each of these effects individually slows down the cooling of Europa and delays the crystallization of the ocean. In this section, we use the method detailed in Section 2 to quantify these effects, and we compare our results with estimates from geological surface observation.

3.1. Ice Shell Properties at 4.55 Gyr

We first run calculations with constant tidal heating, varying the ice reference viscosity, η_{ref}, internal heating and ocean composition within their possible ranges. Figure 3 plots the thicknesses of the whole ice shell and of the stagnant lid after 4.55 Gyr of evolution as a function of the tidal power, and for different values of η_{ref}. Two initial compositions of the ocean are considered: pure water (Figures 3a and 3c), and an initial mix of water and ammonia (NH_3) with initial volume fraction of NH_3, x_{NH3}, equal to 3.0% (Figures 3b and 3d). The impact of ocean composition on the ice shell and stagnant lid thicknesses at 4.55 Gyr is further illustrated in Figure S2 in Supporting Information S1. For the pure water scenario (Figure 3a), and assuming that there is no internal heat within the ice shell ($P_0 = 0$), the ocean crystallizes completely (the ice shell is 161 km thick) for all the values of η_{ref} in the range of 10^{13}–10^{15} Pa·s. Still in the case $P_0 = 0$, incorporating small amounts of NH_3 in the ocean (Figure 3b and Figure S2 in Supporting Information S1) prevents the full crystallization of the ocean. For instance, taking $x_{NH3} = 3.0\%$, a subsurface ocean is maintained whatever the values of η_{ref} we assumed (Figure 3b). A subsurface ocean can also be maintained for lower values of x_{NH3}, around 0.5 vol% (Figure S2 in Supporting Information S1). The presence of subsurface ocean results from the fact that as the ice shell crystalizes, ammonia remains in the ocean and its concentration increases, reducing the ocean liquidus (and thus the temperature at the bottom of the ice shell). As noted earlier, this opposes the crystallization for two reasons: first, the conditions for pursuing crystallization are more difficult to reach; and second, the temperature of the shell is reduced, increasing the viscosity of this shell and weakening convection within it. In all cases, however, the ice shell is very thick compared to the values estimated from surface geological features. For $x_{NH3} = 3.0\%$, it ranges from 110 km (at 10^{15} Pa·s) to about 140 km (at 10^{13} Pa·s).

Dissipating tidal heat within the ice shell has a strong impact on the evolution of this shell (Figures 3a and 3b). For a pure water ocean and $\eta_{ref} = 10^{13}$ Pa·s, a subsurface ocean can be maintained if the tidal power is larger than 1.3 TW. Increasing η_{ref} to 10^{14} Pa·s, the minimum tidal power needed to maintain a subsurface ocean drops to 0.5 TW, and a tidal power of 1.0 TW leads to a 40 km thick ice shell. The initial composition of the ocean still plays a significant role, but to a lesser extent compared to tidal heating and reference viscosity (Figure S2 in Supporting Information S1). For instance, assuming $P_0 = 1.0$ TW and $\eta_{ref} = 10^{14}$ Pa·s, the ice shell thickness is

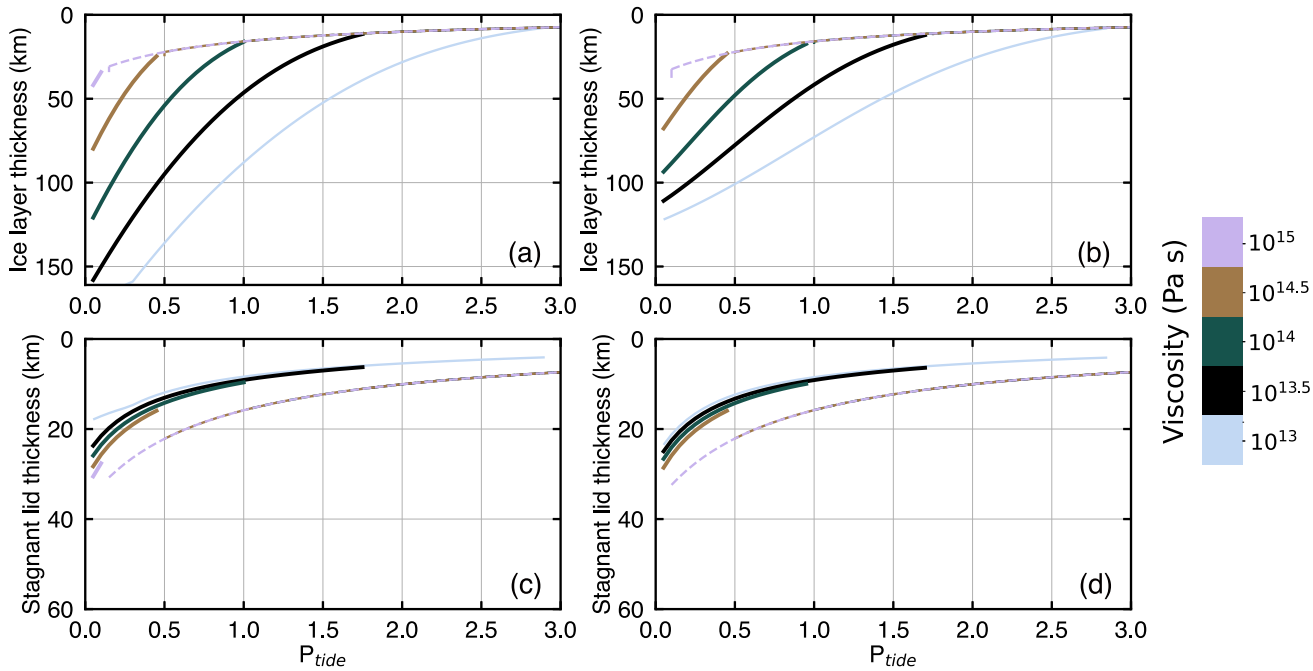

Figure 3. Thickness of ice shell (a) and (b) and stagnant lid (c) and (d) at 4.55 Gyr as a function of the tidal power and for six values of the reference viscosity η_{ref} (Pa·s). Two initial compositions of the ocean are considered: (a) and (c) pure water, and (b) and (d) water plus an initial volume fraction of ammonia equal to 3.0 vol% ammonia. The dashed parts of the curves indicate that the system is not animated by convection.

now equal to 33 km (compared to 40 km for a pure water ocean, and 143 km for $P_0 = 0$). Overall, Figure 3 and Figure S2 in Supporting Information S1 suggest that the presence of impurities in the ocean has a weaker impact on the ice shell evolution than the value of η_{ref} and the amount of tidal heating. We will discuss the influence of ammonia concentration more in details in Section 3.3.3. For all other calculations, we fixed the initial fraction of ammonia to 1.5 vol%.

In our approach, the stagnant lid corresponds to the top, rigid part of the ice shell that is not participating in convection. From this point of view, it may be identified with the brittle part of the ice shell, which can be estimated from gravity measurements (Nimmo et al., 2003; Williams & Greeley, 1998) or studies of impact basin morphology (e.g., Schenk, 2002; Wakita et al., 2024). It is also worth reminding that the stagnant lid impacts the heat transfer through the ice shell, with thicker lids reducing the ability of the shell to cool down and remove heat from Europa's interior. For the pure water scenario without tidal heating, the stagnant lid thickness varies from 10 km to over 40 km, depending on the value of η_{ref} (Figure 3c). Adding tidal heating in the system overall leads to thinner lids, but reduces the influence of the reference viscosity on the stagnant lid thickness. For example, at $P_0 = 1$ TW, the stagnant lid thickness is around 8 and 12 km for values of η_{ref} in the range of 10^{13}–10^{14} Pa·s, respectively. For an ocean with an initial fraction of ammonia of 3.0 vol%, the stagnant lid thickness still increases with increasing tidal power but is nearly independent of the reference viscosity.

Interestingly, Figure 3 shows that when tidal heat is accounted for, and depending on the assumed reference viscosity, the modeled thicknesses of the ice shell and of the stagnant lid are close to those estimated from impact basin morphology. For a reference viscosity around 10^{14} Pa·s and tidal heating between 0.6 and 1.0 TW (which is the range calculated by Hussmann and Spohn (2004) based on thermal-orbital coupling calculations and assuming that all the tidal power is dissipated in the ice shell), Figure 3 indicates that the thickness of the outer ice shell should be thinner than 50 km. However, because Europa's ice shell may thicken and thin periodically due to temporal variations in tidal dissipation, the results plotted in Figure 3 do not necessarily represent the current state of this shell. Quantifying the impact of time-dependent tidal power on ice shell's properties provides an estimate of the minimum and maximum thicknesses allowed by thermal evolution models.

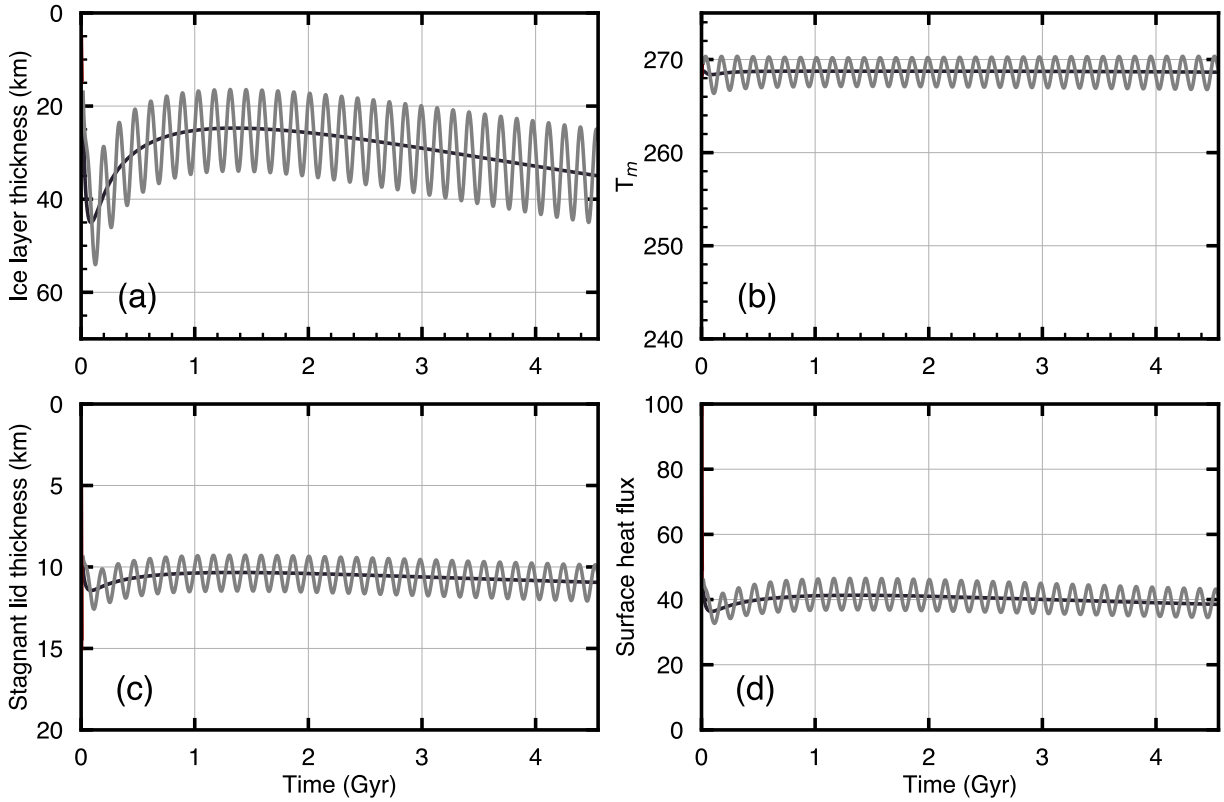

Figure 4. Evolution of (a) the ice shell thickness, (b) the interior temperature, (c) the stagnant lid thickness, and (d) the surface heat flux as a function of time and for reference viscosity $\eta_{ref} = 10^{14}$ Pa·s, initial fraction of ammonia $x_{NH3} = 1.5\%$, and tidal power $P_0 = 1$ TW. The black and gray curves are for constant tidal heating and time-dependent tidal heating with 10% variation in the orbital eccentricity and a 0.14 Gyr period.

3.2. Time-Dependent Variation of Tidal Power

Figure 4 shows the evolution of the ice shell and stagnant lid thickness for constant tidal heating (with $P_0 = 1$ TW) and time-dependent tidal heating corresponding to $P_0 = 1.0$ TW and a 10% variation in orbital eccentricity (i.e., $e_{min} = 0.9\, e_0$ and $e_{max} = 1.1 e_0$ in Equations 17 and 18) with a period of 0.14 Gyr. The reference viscosity and fraction of ammonia are fixed to $\eta_{ref} = 10^{14}$ Pa·s and $x_{NH3} = 1.5\%$, respectively. Figure S3 in Supporting Information S1 further plots the evolution of parameters (bottom temperature and viscosity, concentration of the ocean in ammonia, and mean core temperature) that help to understand the evolution of the shell. Interestingly, through most of the evolution, the viscosity at the bottom of the ice shell remains close to the reference viscosity, and the concentration in ammonia remains around 2.0 vol%. Also, noteworthy, the mean core temperature rises to ~850 K within the first 3 Gyr, and then slowly decreases until 4.55 Gyr.

For a constant tidal heating, the ice shell initially grows until ~0.2 Gyr, reaching a maximum thickness of ~45 km (Figure 4a). The shell then begins to melt, thinning to about 24 km at 1.4 Gyr, and starts to slowly crystallize again after that time. Such a pattern reflects the influence of radiogenic heating within the Europa's core (Figure 2b, red curve), with the radiogenic heat flux peaking at ~1.4 Gyr and decreasing thereafter. At $t = 4.55$ Gyr, the ice shell is about 34 km thick. The thickness of the stagnant lid follows a similar trend over time (Figure 4c), increasing to 11.3 km from 0 to 0.2 Gyr, then thinning to about 10 km at 1.4 Gyr, and slightly thickening again up to 4.55 Gyr.

With variable tidal heating, the ice shell follows a similar trend on average but experiences, in addition, successive cycles of crystallization (thickening) and melting (thinning). Its thickness reaches about 55 km at 0.2 Gyr, and at 1.4 Gyr, it oscillates around the value obtained for constant tidal heating, with minimum and maximum values around 20 and 45 km. Note that the amplitude of these variations slightly increases with time, reaching about 25 km at $t = 4.55$ Gyr. This decrease is again related to the decrease of the radiogenic heat flux after 1.5 Gyr, which allows thicker shells and thus increases the importance of tidal (internal) heating relative to basal heating. Similarly, the thickness of the stagnant lid oscillates from 9.5 to 12 km, maintaining an average thickness

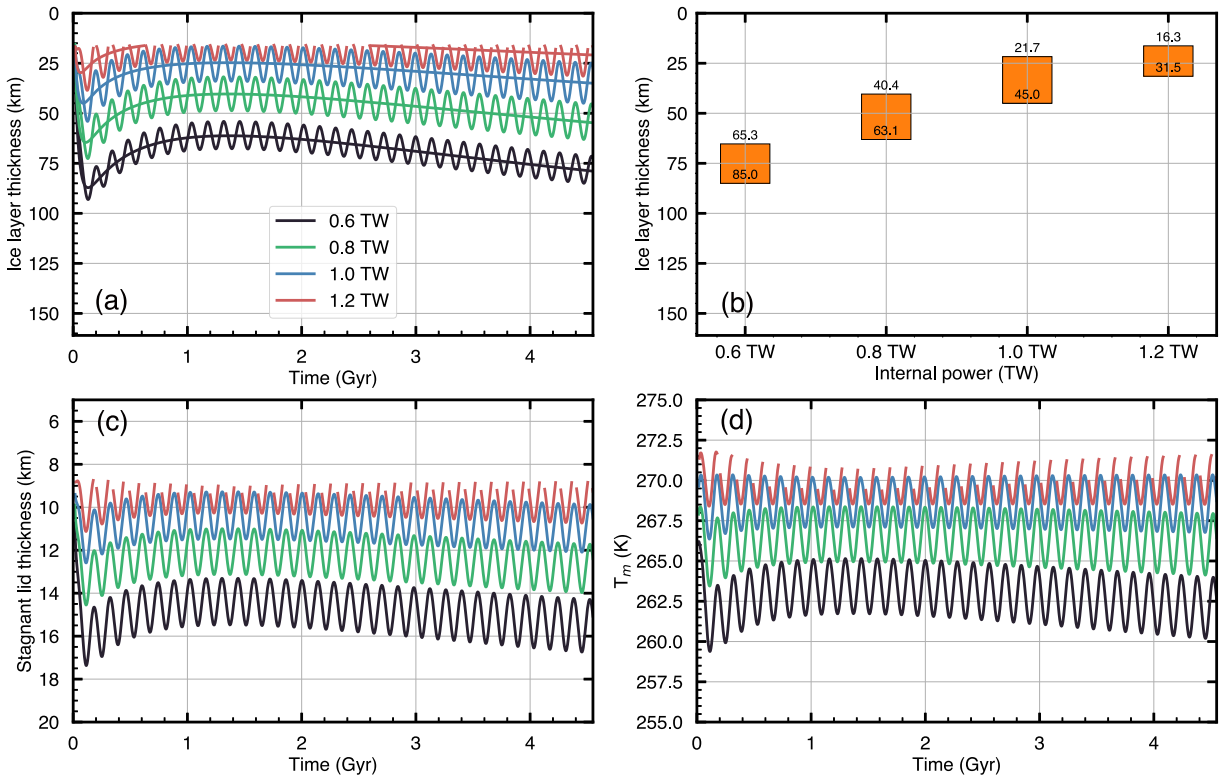

Figure 5. Evolution of the ice shell properties as a function of time for four values of internal power: 0.6, 0.8, 1.0, and 1.2 TW. The ice reference viscosity and initial fraction of ammonia are set to 10^{14} Pa·s and 1.5 vol%, respectively. (a) Ice shell thickness with both constant and time-dependent internal heating. (b) Average amplitude variations of the ice shell thickness over the last 2.5 Gyr. (c) Stagnant lid thickness. (d) Interior temperature. Note that we do not plot the portions where the system is not animated by convection. The legend in plot (a) also applies to plots (c) and (d).

comparable to that obtained for the constant tidal heating scenario. The amplitude of these variations remains around 2 km and again decreases very slightly with time.

While there is, to date, no direct observational constraint on the internal temperature of Europa's ice shell (defined as the average temperature of the well mixed convective interior, i.e., excluding the stagnant lid and the thermal boundary layers) and on the average heat flux at its surface, it is interesting to see how these parameters evolve in our models, as they allow us to better understand the thermal evolution of Europa. The internal temperature (Figure 4b) is nearly constant in time at 268 K, indicating that the system does not cool down. Meanwhile, the surface heat flux (Figure 4d) remains around 40 mW/m^2. Periodic tidal heating induces temperature and heat flux variations of about 4 K and 10 mW/m^2, respectively, that add up to these general trends.

3.3. Influence of Internal and External Factors

In Sections 3.3.1 to 3.3.4, we investigate the effects of internal (tidal heating, ice viscosity and ocean composition) and external (orbital variations) factors on the ice shell evolution and properties. The default values of the tidal power, ice reference viscosity, initial volume fraction of ammonia in the ocean and amplitude variations in Europa's orbital eccentricity are, respectively, fixed to 1.0 TW, 10^{14} Pa·s, 1.5 vol% and 10%, and we successively vary each of these parameters within possible or expected ranges. The period for the changes in orbital eccentricity is fixed at 0.14 Gyr in all calculations. In Section 3.3.5, we further estimate the impact of distributing tidal power between the ice shell and the silicate core.

3.3.1. Internal Heating

We first investigate the influence of the reference tidal power P_0 (Equation 16), which we vary between 0.6 TW and 1.2 TW. Figures 5a and 5b, plotting the evolution of ice shell thickness (for both constant and time-dependent heating) and its time-average over the last 2.5 Gyr, show that the total power exerts a strong control on this

evolution, with greater internal power resulting in a thinner ice shell. For all tested values of the power, the long-term trend is similar to that in Figure 4a, with a maximum thickness around 0.2 Gyr, followed by a melting up to ~1.4 Gyr and a slow re-crystallization from that time up to $t = 4.55$ Gyr. Short cycles of growth and thinning add up to this evolution. The maximum thickness varies between about 95 km for $P_0 = 0.6$ TW and 35 km for $P_0 = 1.2$ TW. After 1.4 Gyr, the ice shell thickens from 60 to 90 km for $P_0 = 0.6$ TW with short scale oscillations around 15 km in amplitude. For $P_0 = 1.0$ TW the thickening is less pronounced and slower, from 20 to 35 km with short scale oscillations around 20 km in amplitude. For $P_0 = 1.2$ TW, the situation is slightly different as convection successively turns on and shuts off. As a result, the thickness of the ice shell remains approximately constant around 25 km during the whole evolution with a reduced oscillation amplitude of about 10 km.

Over time, the evolution of the stagnant lid (Figure 5c) and internal temperature (Figure 5d) are similar to that of the ice shell thickness. The lid grows and the shell cools down from the beginning until 0.2 Gyr. This initial phase is followed by lid thinning and shell warming until 1.4 Gyr, and then slow lid thickening and shell cooling from that time up to $t = 4.55$ Gyr. Increasing tidal heating causes a thinning of the stagnant lid (Figure 5c) and a warming of the ice shell (Figure 5d). For example, for $P_0 = 0.6$ TW, the stagnant lid varies between about 13 and 17 km, while increasing the power to $P_0 = 1.0$ TW results in a thinning of the lid by about 3 km (i.e., the lid thickness is between 9 and 12 km). The interior temperature oscillates between about 260 and 265 K for $P_0 = 0.6$ TW, and increases by 8–15 K for $P_0 = 1.0$ TW. It is worth noting that if the internal power is high enough (e.g., $P_0 = 1.0$ TW and 1.2 TW), the interior temperature remains overall constant (Figure 5d), meaning that the ocean and ice shell are not cooling down. In contrast, for $P_0 = 0.6$ TW and 0.8 TW, the interior temperature decreases over time, reflecting the reduction in radiogenic heat and indicating that the system is cooling down. Finally, the surface heat flux (Figure S4a in Supporting Information S1) is also affected by internal tidal power, with higher tidal power leading to a higher surface heat flux. For example, with a reference tidal power $P_0 = 1.0$ TW, the surface heat flux varies between 35 and 45 mW/m^2, while a tidal power of $P_0 = 0.6$ TW results in surface heat flux oscillating around 25 mW/m^2.

3.3.2. Ice Reference Ice Viscosity

We then investigated the influence of the ice reference viscosity, η_{ref}, which we varied between 10^{13} and 10^{14} Pa·s. Higher values, up to 5 .0× 10^{15} Pa·s, have been considered (Green et al., 2021). Our calculations (Section 3.1, Figure 2) however indicate that if internal heating exceeds 0.6 TW, such high values of η_{ref} result in a purely conductive ice shell during all Europa's evolution. While Europa's ice shell may have experienced purely conductive episodes during its history, surface tectonics suggest that convection has operated and is still likely to operate within it. Therefore, we did not consider values of η_{ref} higher than 10^{15} Pa·s in this study. Figures 6a and 6b show the ice shell thickness evolution and average value in the last 2.5 Gyr. As expected, higher viscosity results in a thinner ice shell. For example, $\eta_{ref} = 10^{13}$ Pa·s leads to an ice shell thickness between about 95 and 115 km over the last 2.5 Gyr, whereas for $\eta_{ref} = 10^{13.5}$ Pa·s, this thickness ranges from about 50 to 80 km. It is interesting to note that the amplitude variations due to orbit's eccentricity are overall larger for thinner shells than for larger shells, with amplitudes of about 17 km for a time-averaged 125 km ice shell, and 22 km for a 60 km shell. This is not a direct effect of the viscosity (or the dissipated tidal power), but results instead from the fact that the tidal heating per mass unit (which is the parameter that affects heat transfer by convection; Section 2.1) is larger in thinner shells. As a consequence, a given change in tidal power results in larger thickness fluctuations in thin shells than in thick shells. In systems experiencing alternating convective and conductive phases, shells are thinner (with average thickness <30 km), and pure conductive conditions limit the minimum shell thickness, therefore reducing the amplitude of its variations.

While the ice shell thins with increasing reference viscosity, the change in stagnant lid thickness appears to be mostly insensitive to these changes in viscosity. Increasing η_{ref} from $10^{13.5}$ Pa·s to 10^{14} Pa·s causes a decrease in stagnant lid thickness by less than 1 km (Figure 6c). For comparison, the variation in the ice shell thickness can exceed 40 km. This reflects the fact that size and strength of the stagnant lid thickness are related to the sensitivity of the viscosity to temperature rather than to the viscosity itself. This explanation also applies to the variations in surface heat flux, which is nearly unchanged when raising the viscosity from 10^{13} to 10^{14} Pa·s (Figure S4b in Supporting Information S1). Finally, Figure 6d shows that a higher η_{ref} results in a higher interior temperature, with the temperature increasing by about 10 K from 10^{13} to 10^{14} Pa·s.

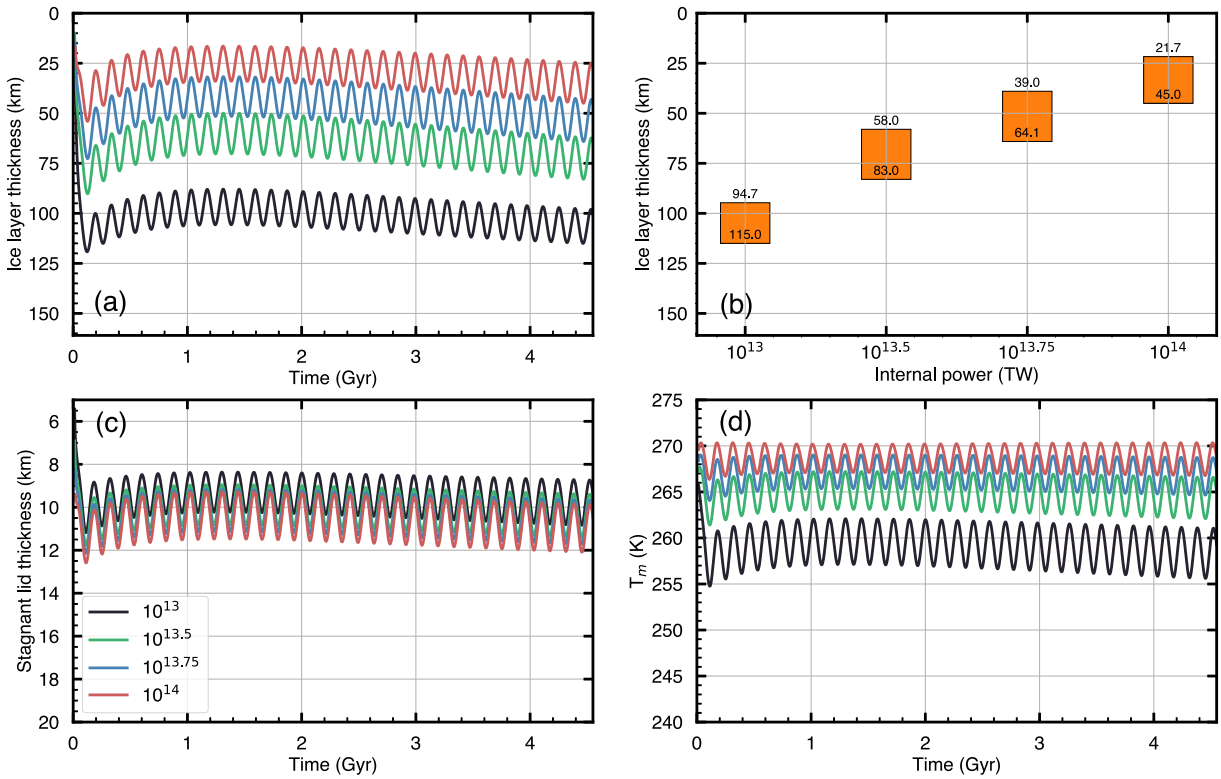

Figure 6. Evolution of the ice shell properties as a function of time for four reference viscosities: 10^{13}, $10^{13.5}$, $10^{13.75}$, and 10^{14} Pa·s. The tidal power and initial fraction of ammonia are set to 1.0 TW and 1.5 vol%, respectively. (a) Ice shell thickness with time-dependent internal heating. (b) Average amplitude variations of the ice shell thickness over the last 2.5 Gyr. (c) Stagnant lid thickness. (d) Interior temperature. Note that we do not plot the portions where the system is not animated by convection. The legend in plot (b) also applies to plots (c) and (d).

3.3.3. Initial Composition of the Subsurface Ocean

Changes in the ice shell thickness trigger changes in the concentration of impurities in the subsurface ocean. As the ice shell thickens, water freezes while impurities remain in the ocean, so that their concentrations increase. Conversely, during periods of thinning, molten ice dilutes the ocean, reducing the concentration of impurities in the seawater. Without tidal heating, the ocean composition has a strong impact on the ice shell evolution (Figure 3 Figure S2 in Supporting Information S1). In particular, compared to a pure water ocean, the presence of ammonia prevents the full crystallization of the ocean. In contrast, if a substantial amount of tidal heating is released in the ice shell, the influence of composition is overwhelmed by the effects of this heating. For a tidal power equal to 1.0 TW, the ice shell thickness remains nearly similar for all the three compositions considered (Figures 7a and 7b). During the last 2.5 Gyr, the average thicknesses are 34, 33.5, and 31 km for pure water and initial NH_3 concentrations of 1.5% and 3.0%, respectively. While the ice shell thickness shows slight thinning with increasing NH_3, the stagnant lid thickness remains, in all cases, largely unaffected by ocean composition (Figure 7c), stabilizing around 11 km at 4.55 Gyr. Likewise, variations in ocean composition do not significantly impact the ice shell internal temperature (Figure 7d) and the surface heat flux (Figure S4c in Supporting Information S1). The decreased influence of ocean composition in the presence of tidal heating can be related to the details of heat transfer through the shell. In the absence of internal heating, the amount of heat that can be extracted from the ocean is controlled by the amplitude of the stagnant lid, which itself depends on the composition of the ocean through its control on the bottom temperature. In contrast, if internal heating is strong enough, plumes are weaker. The heat that can be extracted from the ocean is then limited and controlled by the amount of internal heat. As a result, the composition of the subsurface ocean loses its influence on ice shell evolution.

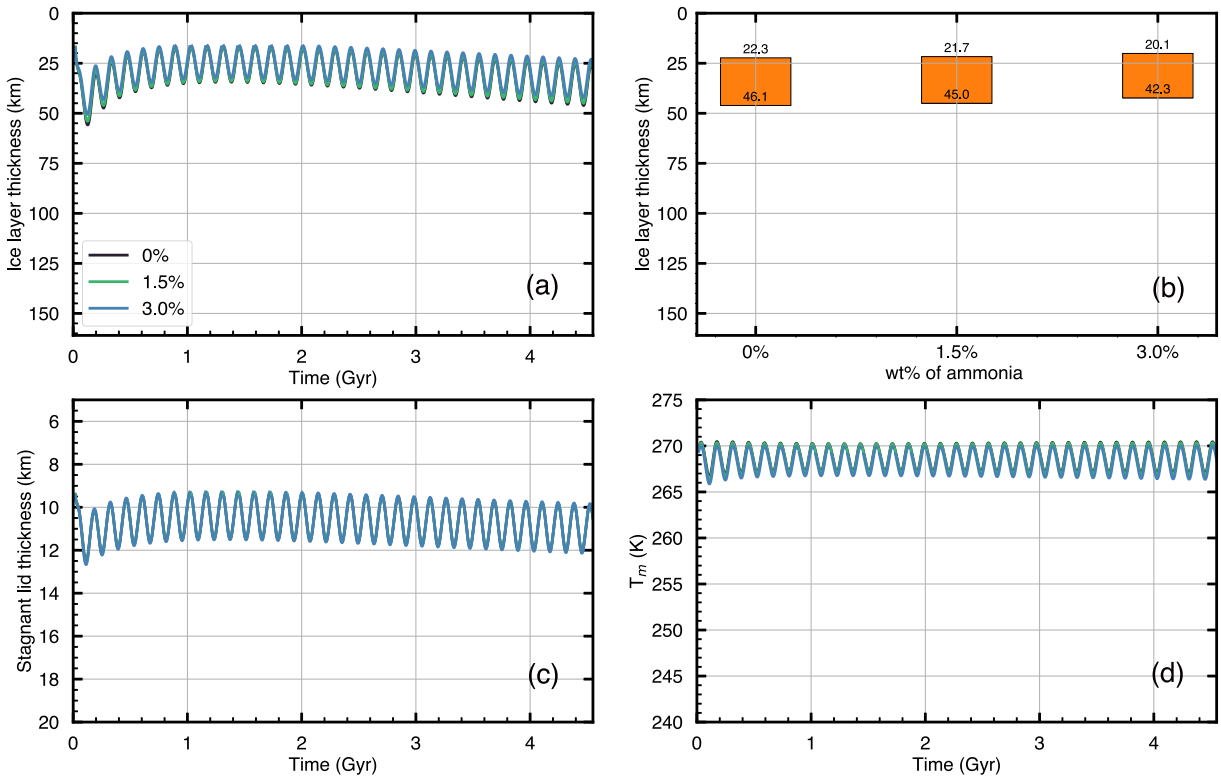

Figure 7. Evolution of the ice shell properties as a function of time for three initial compositions of the initial ocean: pure water, 1.5 vol% of NH_3 and 3.0 vol% of NH_3. The tidal power and reference viscosity are set to 1.0 TW and 10^{14} Pa·s, respectively. (a) Ice shell thickness with time-dependent internal heating. (b) Average amplitude variations of the ice shell thickness over the last 2.5 Gyr. (c) Stagnant lid thickness. (d) Interior temperature. Note that we do not plot the portions where the system is not animated by convection. Note also that, in this case, the curves obtained for different concentrations of ammonia are nearly identical, indicating that when strong tidal heating is present, the influence of ammonia on the ice shell evolution is negligible. The legend in plot (a) also applies to plots (c) and (d).

3.3.4. Influence of Orbital Variations

Currently, Europa's eccentricity is small, at 0.0094, but it has likely varied significantly in the past due to gravitational interactions with Io and Ganymede through the Laplace resonance (e.g., Hussmann & Spohn, 2004; Nimmo et al., 2007; Howell, 2021). Variations in eccentricity affect the intensity of tidal forces exerted on Europa by Jupiter and its other large moons. Changes in these tidal forces result in fluctuations in Europa's deformation, which, in turn, alter frictional heating and Europa's heat budget. In Sections 3.2 and 3.3, we assumed that the amplitude of variations in orbital eccentricity is equal to 10%. Since this amplitude is not well constrained, and to further explore the effects of orbital variations, we conducted additional calculations for eccentricity variations of 5%, 20%, and 50% (Figure 8). For a reference tidal power equal to 1.0 TW, such variations may lead to peak-to-peak variations in tidal heating equal to 1.1025, 1.44, and 2.25 TW, respectively.

Because it triggers substantial changes in the amount of released heat, variations in orbital eccentricity have a strong impact on the ice shell thickness, with larger variations in eccentricity leading to larger changes in this thickness (Figure 8a). For example, with a reference tidal power of 1.0 TW and $\eta_{\text{ref}} = 10^{14}$ Pa·s, a 20% variation in eccentricity results in the ice layer thickness ranging between about 16 and 55 km, whereas a 50% variation in eccentricity leads to thicknesses in the range of 16–83 km (Figure 8b). Since this periodic variation is primarily due to the amplitude variation of tidal heating, its impact on the ice shell is similar to that caused by internal tidal heating (Section 3.3.1). In addition to the ice shell thickness, these variations temporarily affect the stagnant lid thickness (Figure 8c), interior temperature (Figure 8d) and surface heat flux (Figure S4d in Supporting Information S1), with larger eccentricity variations resulting in higher amplitude changes in each ice shell property.

Interestingly, because the variations in Europa's ice shell thickness in response to variations in orbital eccentricity can be large (from ∼14 km and up to 65 km for variation in eccentricity of 5% and 50%, respectively), they introduce a strong variance in the possible ice shell thickness over time. In other words, they may help solve the

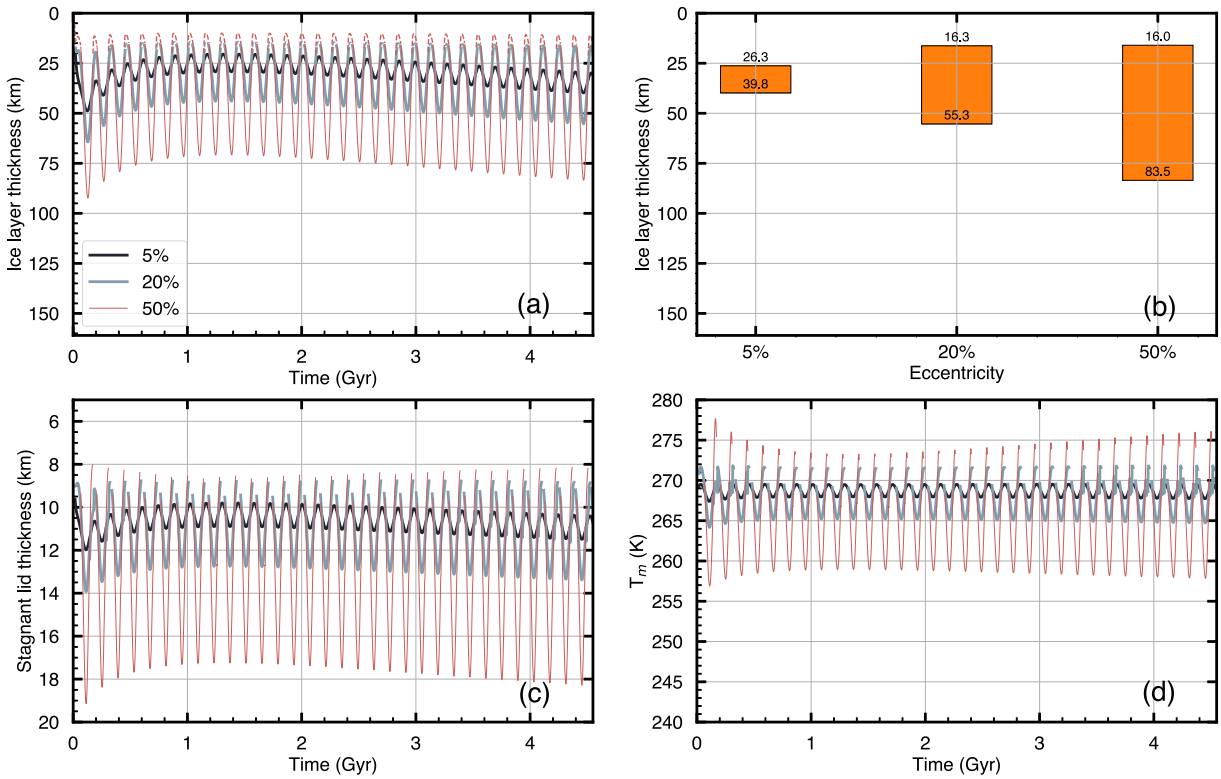

Figure 8. Evolution of the ice shell properties as a function of time with time-averaged internal power $P_0 = 1.0$ TW, reference viscosity $\eta_{ref} = 10^{14}$ Pa·s, and initial ocean ammonia concentration fixed to 1.5%. The amplitude variations of the orbit's eccentricity are set to 5%, 20%, and 50% with a fixed period of 0.14 Gyr. (a) Ice shell thickness. (b) Average amplitude variations of the ice shell thickness over the last 2.5 Gyr. (c) Stagnant lid thickness. (d) Interior temperature. Note that we do not plot the portions where the system is not animated by convection. The legend in plot (a) also applies to plots (c) and (d).

discrepancy between estimates of Europa's ice shell thickness from surface geological features and from thermal modeling methods (see discussion).

3.3.5. Repartition of Tidal Heating

Due to ice properties (viscosity and elastic parameters), viscoelastic deformations of the ice shell are expected to be much larger than in the silicate core and to dissipate more heat. Based on this observation, in all the calculations presented in the previous sections, we assumed that tidal dissipation occurs only within the ice shell. Dissipation in Europa's core may however be stronger than expected. In this section, we investigate the impact of allocating part of the tidal heat in the silicate core. Note that adding too much heat to the core may lead to its partial melting. To avoid this, we estimated the percentage of tidal heating that should not be exceeded to avoid core melting (Figure S5 in Supporting Information S1), assuming that the composition of the silicate layer is similar to that of pyrolite, and using the experimental results of Pierru et al. (2022) to define the melting point of the silicate layer. For instance, if the total tidal dissipation exceeds 0.5 TW, the tidal heating in the silicate core should not exceed 0.1 TW (i.e., 20% of the total power) to avoid melting.

Imposing less heat in the ice shell and adding some in the silicate core allows convection in the shell to extract more heat from the ocean. Meanwhile, it increases the heat available at the bottom of the ice shell. To determine which of these two effects is dominant, we conducted calculations for fractions of tidal power within the ice shell, x_{tide}^{ice}, equal to 85%, 90%, 95%, and 100%, and for two values of the total power 0.6 TW and 1.0 TW. The reference viscosity was set to 10^{14} Pa·s and the initial fraction of ammonia to 1.5%. For these values, our calculations indicate that partitioning tidal heat within the core and the ice shell has only a small effect on the thickness of the ice shell (Figure 9). For total power 0.6 TW (Figure 9 solid lines), a higher proportion of internal heat in the ice shell leads to a thinner ice layer with higher temperatures (Figure S6 in Supporting Information S1) prior to ∼2.5 Gyr, indicating that distributing part of the total tidal heat in the core slightly improves the cooling of

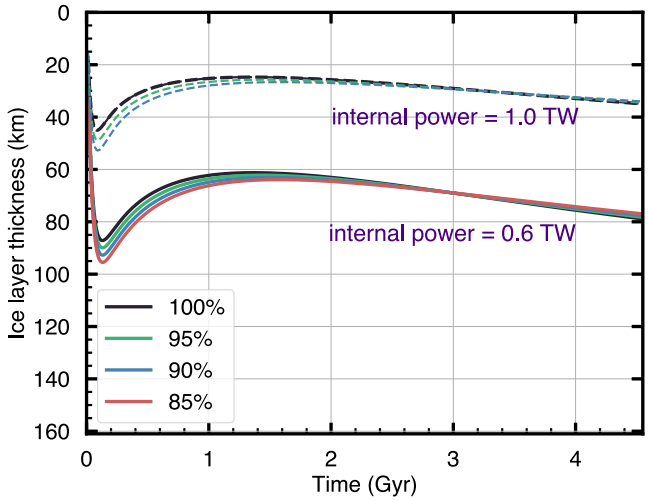

Figure 9. Evolution of the ice shell thickness as a function of time for several repartitions of the tidal heating between the ice shell and the core (with dissipated fraction in the shell equal to 100%, 95%, 90%, and 85%). Tidal heating is constant in time, and two values are considered: 0.6 TW and 1.0 TW. The ice reference viscosity is $\eta_{ref} = 10^{14}$ Pa·s and the initial fraction of ammonia $x_{NH3} = 1.5$ vol%.

Europa. Subsequently, from 2.5 to 4.55 Gyr, as the core cooling rate decreases, the evolution trend reverses, and increased tidal dissipation in the silicate layer results in a thinner ice shell, indicating that the cooling of the shell is now slower due to reduced convection efficiency. We observe a similar evolution for a total power of 1.0 TW, except that the transition time now occurs at approximately 3 Gyr (Figure 9 dashed lines). Note that, in this case, because imposing 10% or more of the tidal heating within the silicate core may lead to core partial melting of this core (Figure S5 in Supporting Information S1), we limited our calculations to values of x_{tide}^{ice} lower than 90%.

4. Discussion

In this study, we investigated the effects of internal (subsurface ocean composition, tidal heating and ice reference viscosity) and external (orbital variations) factors on the evolution of Europa's ice shell properties (total thickness, interior temperature and stagnant lid thickness). Our models indicate that, while the intrinsic effects of the ocean composition on these evolutions are significant, they are of second order compared to the amount of tidal heating and to the value of the ice viscosity, which strongly affect the ice shell thickness and interior temperature. Additionally, because they trigger periodical changes in the amount of tidal heat released, orbital variations significantly affect these properties over time.

In addition to quantitatively investigate the effects of various parameters on Europa's ice properties, our study provides new insights that help to reconcile the values of the ice shell and stagnant lid thicknesses deduced from observational features, most particularly the morphology of large impact basins, with those predicted by thermal evolution models. The different methods used to estimate these thicknesses exhibit different sensitivity to the ice shell thickness at different time and spatial scales. Thermal evolution modeling addresses long-term variations and predicts ice shell thicker than 20 km (Billings & Kattenhorn, 2005), and up to 50–90 km (Vilella et al., 2020), which is larger than estimates based on the analysis of surface geology features. By accounting for temperature and heat flux scaling that specifically accounts for the effects of internal heating on heat transfer within the ice shell (Deschamps & Vilella, 2021), and by considering the variability induced by periodical changes in orbital eccentricity, our calculations lead to a range of ice shell thickness notably smaller than that predicted by previous models of thermal evolution. For values of η_{ref} around 10^{14} Pa·s and tidal power between 0.6 and 1.0 TW, which are well within the expected range for these parameters, the ice shell thickness predicted by our calculations align well with those of Howell (2021), between 23 and 47 km with the best solution at 24.2 km, and with studies based on the morphology of large impact basins, which report ice shell thicker than 20 km, including a conductive lid of about 8 km at its top (Schenk, 2002; Wakita et al., 2024). By contrast, our estimates are still one or two orders of magnitude too large compared to estimates based on lithospheric flexure under loading (Billings & Kattenhorn, 2005 and references therein). However, it should be reminded that these estimates measure the elastic thickness of the ice shell and may reflect the depth of a specific viscosity level, which is equivalent to a specific isotherm. The elastic thickness is thus necessarily thinner than the whole lithosphere (the rigid part of the ice shell), and further thinner than the total ice shell, if a viscous layer is present beneath the rigid shell. Our estimates are also still larger than the thickness deduced from ice raft isostasy, which usually predicts values in the range of 2–6 km (Billings & Kattenhorn, 2005 and references therein). These methods provide the total thickness but are applied to limited areas and chaotic terrains, and rely on estimates of the ice raft height. It cannot be excluded that these rafts do not directly float on the subsurface ocean but rather on pockets of melt located near the top of the shell and triggered by the ascent of a thermal plume rising through a thicker ice shell (Schmidt et al., 2011).

To further illustrate the range of reference viscosity and tidal power that provides good agreement with impact basin morphology estimates, we plotted the average and minimum ice shell and stagnant lid thicknesses over the last 0.5 Gyr as a function of these two parameters and for a 10% variation in orbital eccentricity and a 1.5 vol% initial concentration in ammonia (Figure 10). Differences between average and minimum thicknesses are small (~5 km and less) and are plotted on Figure S7 in Supporting Information S1. Our calculations predict ice shell thickness as low as 15 km for a tidal power of 1.2 TW and an ice reference viscosity of 10^{14} Pa·s or larger. A whole

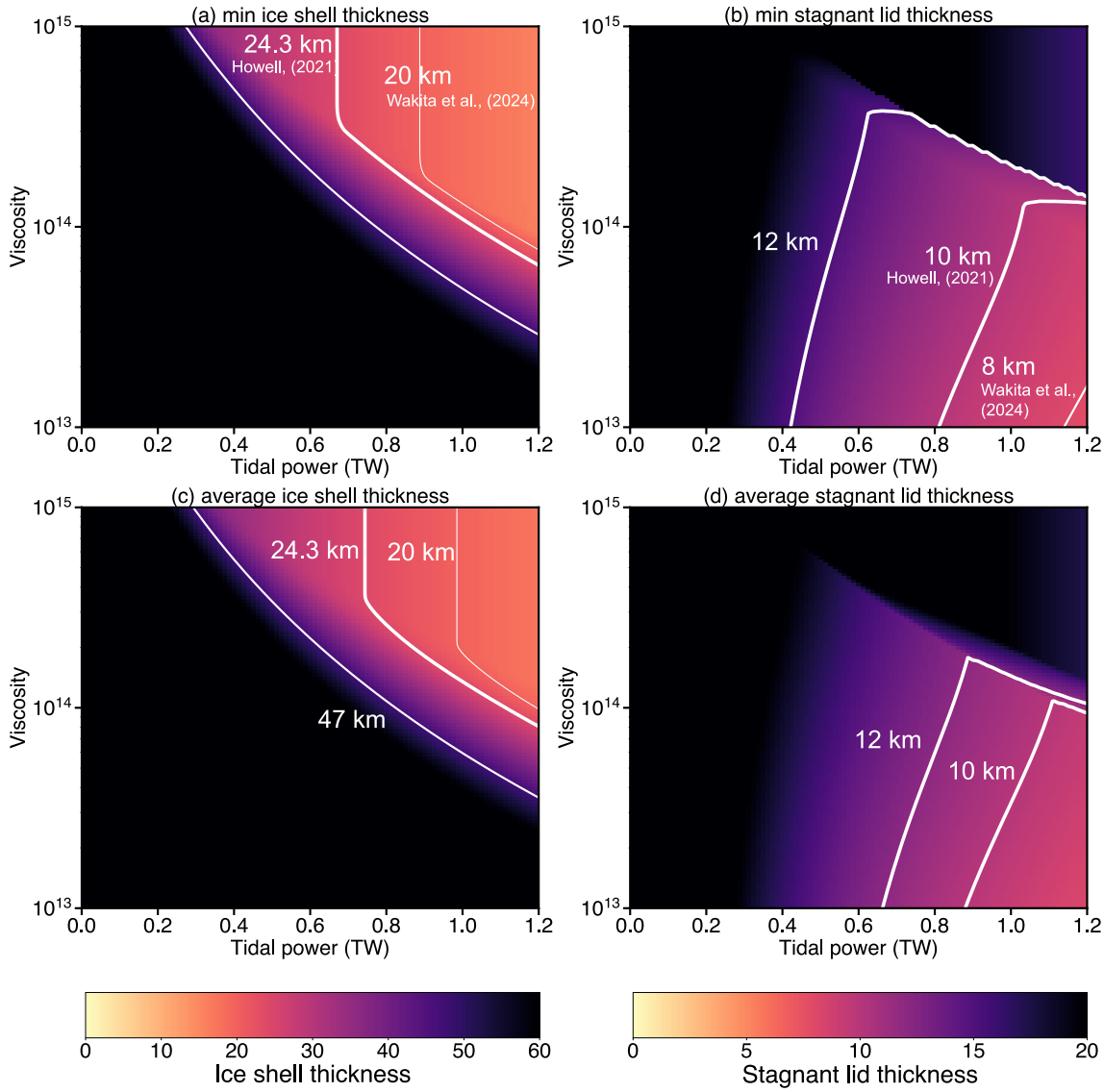

Figure 10. Minimum (a) and (b) and average (c) and (d) ice shell and stagnant lid thicknesses over the past 0.5 Gyr as a function of viscosity and tidal heating. The initial volume fraction of ammonia was set to 1.5% vol of ammonia and the amplitude of variations in orbit's eccentricity to 10%. The color scale is saturated at 80 km for clarity, but in some regions, the actual ice shell thickness can reach up to 161 km (full crystallization). Values beyond 80 km are shown in the same dark blue shade. Differences between the average and minimum thicknesses are shown in Figure S7 in Supporting Information S1.

range of tidal power and viscosity, from 0.6 TW and $10^{14.5}$ Pa·s to 1.2 TW and $10^{13.75}$ Pa·s, explain the best solution proposed by Howell (2021) at 24.2 km. Similarly, our models can fit the range of thicknesses deduced by Wakita et al. (2024), 20−47 km, for a large range of tidal power and reference viscosities, from 0.4 TW and 10^{15} Pa·s to 1.2 TW and $10^{13.5}$ Pa·s. Note that larger variations in eccentricity would provide even more solutions.

The stagnant lid considered in our model corresponds to a rigid lid overlaying a viscous interior and may be associated with the elastic thickness estimated by some studies. Early gravity measurement (Nimmo et al., 2003; Williams & Greeley, 1998) and impact cratering analyses (Moore et al., 1998, 2001; Schenk, 2002; Silber & Johnson, 2017; Wakita et al., 2024) studies suggest that the elastic ice shell thickness may range from 0.5 to 8 km. Using a two-layered model to calculate heat flux balance, Howell (2021) suggested that the lid may be thicker, between 8.5 and 20 km, with a best solution of 10.4 km. Overall, our models predict a rather thick stagnant lid, in the upper end of previous estimates, but still agree with these estimates for reasonable values of the ice viscosity and tidal power (Figure 8a). For instance, a tidal power of 1.0 TW together with a reference viscosity of 10^{14} Pa·s satisfies the optimal solution (i.e., 10.4 km) proposed by Howell (2021). If the model aims to produce a thinner

conductive lid, the reference viscosity would need to be lower than 10^{14} Pa·s. However, this would result in a significant increase in ice shell thickness. One may, however, point out that the presence of a thick, rigid lid at the top of Europa's ice shell is inconsistent with Europa's geologically young surface and tectonic activity. First, it should be noted that a stagnant lid does not preclude the presence of surface tectonic features, as shown, for instance, in the case of Mars. In the case of Europa, partial melting at the base or within the lid due, for instance, to the arrival of hot plumes, may lead to the formation of chaotic terrains such as those observed at Europa's surface (Schmidt et al., 2011; Sotin et al., 2002). Furthermore, it cannot be excluded that Europa experiences an episodic lid regime, in which the lithosphere follows cycles of growth, weakening, and overturn (e.g., Lourenço & Rozel, 2023). In the case of rocky planets (e.g., Venus), such a regime may be triggered by the transition from basalt to eclogite or by increasing stress as the lithosphere thickens. In Europa, tidal heating and its time variations may lead to an episodic lid regime: if too large, heating may weaken this lithosphere to the point that it becomes unstable.

Our models include several simplifications that may further affect Europa's evolution. First, and most importantly, a comprehensive understanding of Europa's ice shell evolution requires coupling its orbital and thermal evolutions to fully capture the variations in tidal heating over time. Such a coupling is not included in our calculations. While the effects of lateral viscosity variations are accounted for through the scaling laws we used (since these relationships do not depend on the viscosity distribution within the ice shell; Deschamps & Vilella, 2021), changes in the amount of tidal heating due to the evolution of the radial structure and viscosity are not accounted for in our calculations. Interestingly, our results show that for dissipated power around 0.6 TW or more and a 10% variation in eccentricity, the change in thickness during the past 3 Gyr is limited to 25 km or less. This may slightly moderate the impact of the changes in ice shell thickness variations on the variations in tidal heating. Over time, the ice shell cooling should lead to an overall increase in the shell viscosity and lead to a slight decrease in tidal dissipation, as that imposed in the models of Běhounková et al. (2021). If internal heat were to decrease, it could lead to a slight thickening of the ice shell compared to our estimates. In addition, the periodic eccentricity variations we impose do not capture all the complexity of Europa's orbital variations, and a more realistic orbital evolution requires taking into account the complexities of the interaction between Europa, Io and Ganymede. Similarly, we did not consider variations in nonsynchronous rotation or physical libration (wobble about the sub-Jupiter point). Overall, while our calculations do not capture all the complexity of the tidal heat release, they may provide a reasonable approximation allowing us to assess the impact of tidal heating on the evolution of Europa's ice shell.

Second, we did not consider temperature-dependent thermal conductivity in our model. Typically, thermal conductivity varies as the inverse of temperature. While temperature-dependent thermal conductivity has a limited influence on the global thermal evolution, it may lead to a thicker stagnant lid (by up to ∼10 km), and a slightly lower interior temperature compared to models with constant thermal conductivity (Deschamps, 2020). However, the impact of temperature-dependent thermal conductivity on the outer shell evolution remains overall very limited and may not alter our main findings and conclusions.

We also did not consider the possible presence of pockets of partial melt within the ice shell. Such pockets could be the source of surface cryo-volcanism and may occur at the base of the stagnant lid, where plumes head are spreading (Vilella et al., 2020), and may reduce tidal dissipation and density within these regions. However, because such reductions would be very local, they may not substantially impact the total amount of heat released, and should be much smaller than the range of dissipated power we explored (0.6–1.2 TW), such that their effect would be implicitly accounted for in our calculations. In addition, Vilella et al. (2020) suggested that the global heat budget would remain largely unaffected by changes in buoyancy and viscosity caused by the presence of melt.

Our approach is a 1D approach, and thus it does not consider a possible dependence of tidal dissipation on latitude and its associated spatial effects on the ice shell thickness. It is generally believed that tidal forces, and thus tidal dissipation, are stronger at higher latitudes (Běhounková et al., 2021; Ojakangas & Stevenson, 1989). However, estimates of surface temperatures across Europa's ice shell contradict this assumption, with equatorial regions being about 50 K warmer than high-latitude regions (Green et al., 2021). Ojakangas and Stevenson (1989) estimated the global distribution of strain rates caused by tidal forces in Europa's shell and calculated associated tidal heating variations with longitude and latitude, allowing for estimations of global variations in ice shell thickness. Current observational evidence (Nimmo et al., 2007) suggests that lateral variations in Europa's ice shell are relatively small, with thickness changes not exceeding 7 km, which is smaller than the temporal variations in our model.

Another possible source of uncertainty is the assumption that the rheology of I_h follows a diffusion creep mechanism and the use of a linearized temperature-dependent viscosity (Frank-Kamenetskii approximation) law to build heat flux and interior temperature scaling Deschamps and Vilella (2021). Harel et al. (2020) considered a composite viscosity law that includes diffusion creep, grain boundary sliding, basal slip and dislocation creep. Their results suggested that the Frank-Kamenetskii approximation overestimates the efficiency of heat transfer by up to 30% compared to the Arrhenius law for a diffusion creep regime, leading to higher heat flux, thicker ice shell and thinner stagnant lid. Our estimates of Europa's ice shell thickness may thus be understood as upper bound values, and the effect of a complex rheology should result in thinner ice shells, further reconciling geological and modeled estimates of this thickness. Additional calculations incorporating a complex rheology are nevertheless required to quantitatively estimate their impact.

Finally, we did not account for the presence of a layer of volatiles or gas hydrates at the base of the ice shell, as hypothesized by Kamata et al. (2019) in the case of Pluto. Such a layer may result from the simultaneous crystallization of water and impurities as the eutectic composition in the subsurface ocean is reached. Due to its lowered thermal conductivity, this layer may act as a thermal insulator, preventing the crystallization of the ocean and limiting the ice shell thickness. If such a layer is present, our estimates of the ice shell thickness may again be seen as upper limits, and accounting for its presence would further improve the agreement between geological and modeled estimates, or allow agreement for wider ranges of tidal power and reference viscosities.

5. Conclusions and Perspectives

Our study provides quantitative constraints on the time-dependent variations in Europa's outer ice shell properties, including its total thickness and the thickness of its brittle upper layer. These changes are driven by variations in the amount of tidal heating in response to changes in orbital eccentricity. Interestingly, our results, which suggest an ice shell thickness in the range of 20–45 km, are in agreement with estimates of Europa's ice shell thickness derived from the morphology of large impact basins. Our findings may be helpful in interpreting future spacecraft observations. For instance, gravity measurements from Europa Clipper are expected to estimate the k_2 Love number (Mazarico et al., 2023), which, based on our modeled ice shell thickness, should be in the range of 0.22–0.24. Furthermore, the Europa Clipper radar experiment (Blankenship et al., 2024) will be able to detect an ice/ocean boundary up to a depth of 30 km, which lies well within the thickness range predicted by our calculations. Additionally, our modeling approach offers insights into the dynamic environment and potential internal structure of other icy moons, particularly Ganymede and Callisto around Jupiter, Titan and Enceladus around Saturn, as well as the moons of Uranus and Neptune. Extending this approach to these bodies may improve our understanding of the geophysical processes that affect or have affected their evolution. Based on our calculations, a general conclusion is that the presence of impurities is likely to allow the persistence of a subsurface ocean beneath the outer ice shell, even if tidal heating is limited or absent. The thickness of the outer shell (or, equivalently, of the ocean) is, however, controlled by the amount of tidal heating, with strong heating leading to thin ice shells (typically ∼30 km for Europa), and moderate or low heating, as in the case of Ganymede, resulting in much thicker ice shells.

Conflict of Interest

The authors declare no conflicts of interest relevant to this study.

Data Availability Statement

All data are generated by calculations using a method that is fully described in the article. The data used for generating the figures displayed in this article and the code used to compute these data are freely available for academic purposes and are available from https://zenodo.org/records/15572984 (Chen et al., 2025).

Acknowledgments
This work was partially supported by the Academia Sinica and the National Science and Technology Council (NSTC) of Taiwan, under Contract AS-IA-113-M02 and 112-2116-M-001-029 (FD) and AS-IA-111-M02 and NSTC 113-2628-M-001-013 (WPH).

References

Allu Peddinti, D., & McNamara, A. K. (2019). Dynamical investigation of a thickening ice-shell: Implications for the icy moon Europa. *Icarus*, *329*, 251–269. https://doi.org/10.1016/j.icarus.2019.03.037

Anderson, J. D., Schubert, G., Jacobson, R. A., Lau, E. L., Moore, W. B., & Sjogren, W. L. (1998). Europa's differentiated internal structure: Inferences from four galileo encounters. *Science*, *281*(5385), 2019–2022. https://doi.org/10.1126/science.281.5385.2019

Becker, T. M., Zolotov, M. Y., Gudipati, M. S., Soderblom, J. M., McGrath, M. A., Henderson, B. L., et al., Europa Clipper Composition Working Group. (2024). Exploring the composition of Europa with the upcoming Europa Clipper mission. *Space Science Reviews*, *220*(5), 49. https://doi.org/10.1007/s11214-024-01069-y

Běhounková, M., Tobie, G., Choblet, G., & Čadek, O. (2010). Coupling mantle convection and tidal dissipation: Applications to Enceladus and earth-like planets. *Journal of Geophysical Research*, *115*(E9), 2009JE003564. https://doi.org/10.1029/2009JE003564

Běhounková, M., Tobie, G., Choblet, G., Kervazo, M., Melwani Daswani, M., Dumoulin, C., & Vance, S. D. (2021). Tidally induced magmatic pulses on the Oceanic floor of Jupiter's moon europa. *Geophysical Research Letters*, *48*(3), e2020GL090077. https://doi.org/10.1029/2020GL090077

Beuthe, M. (2015). Tides on Europa: The membrane paradigm. *Icarus*, *258*, 109–135. https://doi.org/10.1016/j.icarus.2014.10.027

Billings, S. E., & Kattenhorn, S. A. (2005). The great thickness debate: Ice shell thickness models for Europa and comparisons with estimates based on flexure at ridges. *Icarus*, *177*(2), 397–412. https://doi.org/10.1016/j.icarus.2005.03.013

Blankenship, D. D., Moussessian, A., Chapin, E., Young, D. A., Wesley Patterson, G., Plaut, J. J., et al. (2024). Radar for europa assessment and sounding: Ocean to near-surface (REASON). *Space Science Reviews*, *220*(5), 51. https://doi.org/10.1007/s11214-024-01072-3

Buffo, J. J., Schmidt, B. E., Huber, C., & Meyer, C. R. (2021). Characterizing the ice-ocean interface of icy worlds: A theoretical approach. *Icarus*, *360*, 114318. https://doi.org/10.1016/j.icarus.2021.114318

Carlson, R. W. (1999). A Tenuous carbon dioxide atmosphere on Jupiter's Moon Callisto. *Science*, *283*(5403), 820–821. https://doi.org/10.1126/science.283.5403.820

Carr, M. H., Belton, M. J. S., Chapman, C. R., Davies, M. E., Geissler, P., Greenberg, R., et al. (1998). Evidence for a subsurface ocean on Europa. *Nature*, *391*(6665), 363–365. https://doi.org/10.1038/34857

Chen, J.-C., Deschamps, F., & Hsieh, W.-P. (2025). Temporal changes in Europa's ice shell thickness: Insights from models of convection (v2) [Dataset]. *Zenodo*. https://doi.org/10.5281/zenodo.15572984

Davaille, A., & Jaupart, C. (1993). Transient high-rayleigh-number thermal convection with large viscosity variations. *Journal of Fluid Mechanics*, *253*(1), 141–166. https://doi.org/10.1017/S0022112093001740

Deschamps, F. (2020). Stagnant lid convection with temperature-dependent thermal conductivity and the thermal evolution of icy worlds. *Geophysical Journal International*, *224*(3), 1870–1889. https://doi.org/10.1093/gji/ggaa540

Deschamps, F., & Lin, J.-R. (2014). Stagnant lid convection in 3D-Cartesian geometry: Scaling laws and applications to icy moons and dwarf planets. *Physics of the Earth and Planetary Interiors*, *229*, 40–54. https://doi.org/10.1016/j.pepi.2014.01.002

Deschamps, F., & Sotin, C. (2001). Thermal convection in the outer shell of large icy satellites. *Journal of Geophysical Research*, *106*(E3), 5107–5121. https://doi.org/10.1029/2000JE001253

Deschamps, F., Tackley, P. J., & Nakagawa, T. (2010). Temperature and heat flux scalings for isoviscous thermal convection in spherical geometry: Thermal convection scalings in spherical geometry. *Geophysical Journal International*. no-no. https://doi.org/10.1111/j.1365-246X.2010.04637.x

Deschamps, F., & Vilella, K. (2021). Scaling laws for mixed-heated stagnant-lid convection and application to europa. *Journal of Geophysical Research: Planets*, *126*(10), e2021JE006963. https://doi.org/10.1029/2021JE006963

Durham, W. B., Prieto-Ballesteros, O., Goldsby, D. L., & Kargel, J. S. (2010). Rheological and thermal properties of icy materials. *Space Science Reviews*, *153*(1–4), 273–298. https://doi.org/10.1007/s11214-009-9619-1

Gaidos, E. J., & Nimmo, F. (2000). Tectonics and water on Europa. *Nature*, *405*(6787), 637. https://doi.org/10.1038/35015170

Goldsby, D. L., & Kohlstedt, D. L. (2001). Superplastic deformation of ice: Experimental observations. *Journal of Geophysical Research*, *106*(B6), 11017–11030. https://doi.org/10.1029/2000JB900336

Gomez Casajus, L., Zannoni, M., Modenini, D., Tortora, P., Nimmo, F., Van Hoolst, T., et al. (2021). Updated Europa gravity field and interior structure from a reanalysis of Galileo tracking data. *Icarus*, *358*, 114187. https://doi.org/10.1016/j.icarus.2020.114187

Grasset, O., & Sotin, C. (1996). The cooling rate of a liquid shell in Titan's interior. *Icarus*, *123*(1), 101–112. https://doi.org/10.1006/icar.1996.0144

Green, A. P., Montesi, L. G. J., & Cooper, C. M. (2021). The growth of europa's icy shell: Convection and crystallization. *Journal of Geophysical Research: Planets*, *126*(4), e2020JE006677. https://doi.org/10.1029/2020JE006677

Han, L., & Showman, A. P. (2010). Coupled convection and tidal dissipation in Europa's ice shell. *Icarus*, *207*(2), 834–844. https://doi.org/10.1016/j.icarus.2009.12.028

Harel, L., Dumoulin, C., Choblet, G., Tobie, G., & Besserer, J. (2020). Scaling of heat transfer in stagnant lid convection for the outer shell of icy moons: Influence of rheology. *Icarus*, *338*, 113448. https://doi.org/10.1016/j.icarus.2019.113448

Hoppa, G. V., Tufts, B. R., Greenberg, R., & Geissler, P. E. (1999). Formation of cycloidal features on europa. *Science*, *285*(5435), 1899–1902. https://doi.org/10.1126/science.285.5435.1899

Howell, S. M. (2021). The likely thickness of Europa's icy shell. *The Planetary Science Journal*, *2*(4), 129. https://doi.org/10.3847/PSJ/abfe10

Hurford, T. A., Beyer, R. A., Schmidt, B., Preblich, B., Sarid, A. R., & Greenberg, R. (2005). Flexure of Europa's lithosphere due to ridge-loading. *Icarus*, *177*(2), 380–396. https://doi.org/10.1016/j.icarus.2005.06.019

Hussmann, H. (2002). Thermal equilibrium States of Europa's ice shell: Implications for internal Ocean thickness and surface heat flow. *Icarus*, *156*(1), 143–151. https://doi.org/10.1006/icar.2001.6776

Hussmann, H., & Spohn, T. (2004). Thermal-orbital evolution of Io and Europa. *Icarus*, *171*(2), 391–410. https://doi.org/10.1016/j.icarus.2004.05.020

Kamata, S., Nimmo, F., Sekine, Y., Kuramoto, K., Noguchi, N., Kimura, J., & Tani, A. (2019). Pluto's ocean is capped and insulated by gas hydrates. *Nature Geoscience*, *12*(6), 407–410. https://doi.org/10.1038/s41561-019-0369-8

Khurana, K. K., Kivelson, M. G., Stevenson, D. J., Schubert, G., Russell, C. T., Walker, R. J., & Polanskey, C. (1998). Induced magnetic fields as evidence for subsurface oceans in Europa and Callisto. *Nature*, *395*(6704), 777–780. https://doi.org/10.1038/27394

Kirk, R. L., & Stevenson, D. J. (1987). Thermal evolution of a differentiated Ganymede and implications for surface features. *Icarus*, *69*(1), 91–134. https://doi.org/10.1016/0019-1035(87)90009-1

Kivelson, M. G., Jia, X., Lee, K. A., Raymond, C. A., Khurana, K. K., Perley, M. O., et al. (2023). The Europa clipper magnetometer. *Space Science Reviews*, *219*(6), 48. https://doi.org/10.1007/s11214-023-00989-5

Kivelson, M. G., Khurana, K. K., Russell, C. T., Volwerk, M., Walker, R. J., & Zimmer, C. (2000). Galileo magnetometer measurements: A stronger case for a subsurface Ocean at europa. *Science*, *289*(5483), 1340–1343. https://doi.org/10.1126/science.289.5483.1340

Lari, G., Saillenfest, M., & Fenucci, M. (2020). Long-term evolution of the Galilean satellites: The capture of Callisto into resonance. *A&A*, *639*, A40. https://doi.org/10.1051/0004-6361/202037445

Lodders, K. (2003). Solar System abundances and condensation temperatures of the elements. *The Astrophysical Journal*, *591*(2), 1220–1247. https://doi.org/10.1086/375492

Lourenço, D. L., & Rozel, A. B. (2023). The past and future of plate tectonics and other tectonic regimes. In J. C. Duarte (Ed.), *Dynamics of Plate tectonics and mantle convection* (pp. 181–196). Elsevier. https://doi.org/10.1016/B978-0-323-85733-8.00004-4

Mazarico, E., Buccino, D., Castillo-Rogez, J., Dombard, A. J., Genova, A., Hussmann, H., et al. (2023). The Europa clipper gravity and radio science investigation. *Space Science Reviews*, *219*(4), 30. https://doi.org/10.1007/s11214-023-00972-0

Mc Kinnon, W. B., & Melosh, H. J. (1980). Evolution of planetary lithospheres: Evidence from multiringed structures on Ganymede and Callisto. *Icarus*, *44*(2), 454–471. https://doi.org/10.1016/0019-1035(80)90037-8

Montagnat, M., & Duval, P. (2000). Rate controlling processes in the creep of polar ice, in£uence of grain boundary migration associated with recrystallization. *Earth and Planetary Science Letters*.

Moore, J. M., Asphaug, E., Belton, M. J. S., Bierhaus, B., Breneman, H. H., Brooks, S. M., et al. (2001). Impact features on europa: Results of the Galileo Europa Mission (GEM). *Icarus*, *151*(1), 93–111. https://doi.org/10.1006/icar.2000.6558

Moore, J. M., Asphaug, E., Sullivan, R. J., Klemaszewski, J. E., Bender, K. C., Greeley, R., et al. (1998). Large impact features on europa: Results of the Galileo Nominal Mission. *Icarus*, *135*(1), 127–145. https://doi.org/10.1006/icar.1998.5973

Moresi, L.-N., & Solomatov, V. S. (1995). Numerical investigation of 2D convection with extremely large viscosity variations. *Physics of Fluids*, *7*(9), 2154–2162. https://doi.org/10.1063/1.868465

Mousis, O., Lunine, J. I., Thomas, C., Pasek, M., Marbœuf, U., Alibert, Y., et al. (2009). Clathration of volatiles in the solar nebula and implications for the origin of Titan's atmosphere. *The Astrophysical Journal*, *691*(2), 1780–1786. https://doi.org/10.1088/0004-637X/691/2/1780

Nimmo, F., & Gaidos, E. (2002). Strike-slip motion and double ridge formation on Europa. *Journal of Geophysical Research*, *107*(E4), 5-1–8. https://doi.org/10.1029/2000JE001476

Nimmo, F., Giese, B., & Pappalardo, R. T. (2003). Estimates of Europa's ice shell thickness from elastically-supported topography. *Geophysical Research Letters*, *30*(5), 2002GL016660. https://doi.org/10.1029/2002GL016660

Nimmo, F., Thomas, P., Pappalardo, R., & Moore, W. (2007). The global shape of Europa: Constraints on lateral shell thickness variations. *Icarus*, *191*(1), 183–192. https://doi.org/10.1016/j.icarus.2007.04.021

Ogawa, M., Schubert, G., & Zebib, A. (1991). Numerical simulations of three-dimensional thermal convection in a fluid with strongly temperature-dependent viscosity. *Journal of Fluid Mechanics*, *233*, 299–328. https://doi.org/10.1017/S0022112091000496

Ojakangas, G., & Stevenson, D. J. (1989). Thermal state of an ice shell on Europa. *Icarus*, *81*(2), 220–241. https://doi.org/10.1016/0019-1035(89)90052-3

Pierru, R., Andrault, D., Manthilake, G., Monteux, J., Devidal, J. L., Guignot, N., et al. (2022). Deep mantle origin of large igneous provinces and komatiites. *Science Advances*, *8*(44), eabo1036. https://doi.org/10.1126/sciadv.abo1036

Press, W. H., Flannery, B. P., Teukolsky, S. A., & Vetterling, W. T. (1992). *Numerical Recipes (2nd edtion)*. Cambridge University Press.

Roberts, J. H., McKinnon, W. B., Elder, C. M., Tobie, G., Biersteker, J. B., Young, D., et al. (2023). Exploring the interior of europa with the europa clipper. *Space Science Reviews*, *219*(6), 46. https://doi.org/10.1007/s11214-023-00990-y

Schenk, P. M. (2002). Thickness constraints on the icy shells of the galilean satellites from a comparison of crater shapes. *Nature*, *417*(6887), 419–421. https://doi.org/10.1038/417419a

Schilling, N., Neubauer, F. M., & Saur, J. (2007). Time-varying interaction of Europa with the jovian magnetosphere: Constraint on the conductivity of the ocean sub-surface. *Icarus*, *192*(1), 41–55. https://doi.org/10.1016/j.icarus.2007.06.024

Schmidt, B. E., Blankenship, D. D., Patterson, G. W., & Schenk, P. M. (2011). Active formation of 'chaos terrain' over shallow subsurface water on Europa. *Nature*, *479*(7374), 502–505. https://doi.org/10.1038/nature10608

Schubert, A., & Spohn. (2004). Interior composition, structure and dynamics of the Galilean satellites. In *Jupiter: The planet, satellites and magnetosphere* (Vol. 1, pp. 281–306).

Silber, E. A., & Johnson, B. C. (2017). Impact crater morphology and the structure of Europa's ice shell. *Journal of Geophysical Research: Planets*, *122*(12), 2685–2701. https://doi.org/10.1002/2017JE005456

Sotin, C., Grasset, O., & Beauchesne, S. (1997). Thermodynamic properties of high pressure ices: Implications for the dynamics and internal structure of large icy satellites. In B. Schmitt (Ed.), *Solar System ices* (pp. 79–96). Springer.

Sotin, C., & Labrosse, S. (1999). Three-dimensional thermal convection in an iso-viscous, infinite Prandtl number fluid heated from within and from below: Applications to the transfer of heat through planetary mantles. *Physics of the Earth and Planetary Interiors*, *112*(3–4), 171–190. https://doi.org/10.1016/S0031-9201(99)00004-7

Sotin, C., Sotin, C., Head, J. W., III, & Tobie, G. (2002). Europa: Tidal heating of upwelling thermal plumes and the origin of lenticulae and chaos melting. *Geophysical Research Letters*, *29*(8), 74-1–4. https://doi.org/10.1029/2001GL013844

Trumbo, S. K., Brown, M. E., & Hand, K. P. (2019). H_2O_2 within chaos terrain on Europa's leading hemisphere. *The Astronomical Journal*, *158*(3), 127. https://doi.org/10.3847/1538-3881/ab380c

Tyler, R. T. (2014). Comparative estimates of the heat generated by ocean tides on icy satellites in the outer Solar System. *Icarus*, *243*, 358–385. https://doi.org/10.1016/j.icarus.2014.08.037

Vilella, K., Choblet, G., Tsao, W.-E., & Deschamps, F. (2020). Tidally heated convection and the occurrence of melting in icy satellites: Application to europa. *Journal of Geophysical Research: Planets*, *125*(3), e2019JE006248. https://doi.org/10.1029/2019JE006248

Wakita, S., Johnson, B. C., Silber, E. A., & Singer, K. N. (2024). Multiring basin formation constrains Europa's ice shell thickness. *Science Advances*, *10*(12), eadj8455. https://doi.org/10.1126/sciadv.adj8455

Walker, M. E., & Rhoden, A. (2022). Tidal heating at europa using the multifrequency analysis of tidal heating toolkit. *The Planetary Science Journal*, *3*(7), 149. https://doi.org/10.3847/PSJ/ac6df0

Weertman, J. (1983). Creep deformation of ice. *Annual Review of Earth and Planetary Sciences*, *11*(1), 215–240. https://doi.org/10.1146/annurev.ea.11.050183.001243

Williams, K. K., & Greeley, R. (1998). Estimates of ice thickness in the Conamara Chaos Region of Europa. *Geophysical Research Letters*, *25*(23), 4273–4276. https://doi.org/10.1029/1998GL900144

Yao, C., Deschamps, F., Lowman, J. P., Sanchez-Valle, C., & Tackley, P. J. (2014). Stagnant lid convection in bottom-heated thin 3-D spherical shells: Influence of curvature and implications for dwarf planets and icy moons: Yao et al. *Journal of Geophysical Research: Planets*, *119*(8), 1895–1913. https://doi.org/10.1002/2014JE004653